JCB Journal of Cell Biology

ARTICLE

Deorphanizing FAM19A proteins as pan-neurexin ligands with an unusual biosynthetic binding mechanism

Anna J. Khalaj[1], Fredrik H. Sterky[1], Alessandra Sclip[1], Jochen Schwenk[2], Axel T. Brunger[1], Bernd Fakler[2,3,4], and Thomas C. Südhof[1]

Neurexins are presynaptic adhesion molecules that organize synapses by binding to diverse trans-synaptic ligands, but how neurexins are regulated is incompletely understood. Here we identify FAM19A/TAFA proteins, "orphan" cytokines, as neurexin regulators that interact with all neurexins, except for neurexin-1γ, via an unusual mechanism. Specifically, we show that FAM19A1-A4 bind to the cysteine-loop domain of neurexins by forming intermolecular disulfide bonds during transport through the secretory pathway. FAM19A-binding required both the cysteines of the cysteine-loop domain and an adjacent sequence of neurexins. Genetic deletion of neurexins suppressed FAM19A1 expression, demonstrating that FAM19As physiologically interact with neurexins. In hippocampal cultures, expression of exogenous FAM19A1 decreased neurexin *O*-glycosylation and suppressed its heparan sulfate modification, suggesting that FAM19As regulate the post-translational modification of neurexins. Given the selective expression of FAM19As in specific subtypes of neurons and their activity-dependent regulation, these results suggest that FAM19As serve as cell type–specific regulators of neurexin modifications.

Introduction

Synapses are the basic units of information processing in the brain. Although a fundamental understanding of how synapses transfer and process information has emerged recently, how synapses are formed, maintained, and continuously restructured throughout life remains largely unknown. Synapses are likely controlled at every phase of their life cycle by trans-synaptic adhesion signals, starting with their initial formation and the specification of their properties, and continuing throughout life with their restructuring during synaptic plasticity, but how precisely synaptic adhesion molecules shape synaptic properties remains unclear. Many candidate synaptic adhesion molecules have been described (Jang et al., 2017; Krueger-Burg et al., 2017; Ribic and Biederer, 2019; Südhof, 2018). Among these, neurexins are arguably the best studied (reviewed in Han et al., 2019; Kasem et al., 2018; Reissner et al., 2013; Rudenko, 2019; Südhof, 2017). Despite much work, however, the functions and mechanisms of action of neurexins remain enigmatic.

Accumulating evidence suggests that neurexins play distinct roles at different types of synapses rather than performing a single canonical function at all synapses (e.g., see Anderson et al., 2015; Aoto et al., 2015; Chen et al., 2017). Neurexins are highly conserved type I membrane proteins predominantly localized to presynaptic terminals (Missler et al., 2003; Trotter et al., 2019; Ushkaryov et al., 1992), although astrocytes also express neurexins (Gokce and Südhof, 2013; Tasic et al., 2018; Zeisel et al., 2018). Each of the three vertebrate neurexin genes (*Nrxn1-3*) produces two isoforms (α- and β-neurexins) via different promoters (Ushkaryov et al., 1992, 1994). In addition, the neurexin-1 gene contains a third promoter that produces Nrxn1γ (Sterky et al., 2017). α-Neurexins contain six laminin-neurexin-sex hormone-binding globulin (LNS) domains with three interspersed epidermal growth factor (EGF) domains, a juxtamembranous stalk region that includes a cysteine-loop (CysL) domain, a transmembrane region, and a short cytosolic tail containing a PSD-95/Discs-large/ZO-I (PDZ)-binding domain (Gokce and Südhof, 2013; Ushkaryov and Südhof, 1993; Ushkaryov et al., 1992). β-Neurexins possess a unique N-terminal sequence and splice into α-neurexins just N-terminal to the sixth (last) LNS domain (Ushkaryov et al., 1992, 1994). Nrxn1γ also

[1]Department of Molecular and Cellular Physiology, Howard Hughes Medical Institute, Stanford University School of Medicine, Stanford, CA; [2]Institute of Physiology, Faculty of Medicine, University of Freiburg, Freiburg, Germany; [3]Centres for Biological Signalling Studies (BIOSS) and Integrative Biological Signalling Studies (CIBSS), Freiburg, Germany; [4]Center for Basics in NeuroModulation, Freiburg, Germany.

Correspondence to Anna J. Khalaj: ajkhalaj@stanford.edu; Thomas C. Südhof: tcs1@stanford.edu; F.H. Sterky's present address is Department of Laboratory Medicine and Wallenberg Centre for Molecular and Translational Medicine, University of Gothenburg, Gothenburg, Sweden.

contains a unique N-terminal sequence that is followed by part of the stalk region (Sterky et al., 2017). Due to the usage of up to six canonical sites of alternative splicing and three different promoters, thousands of neurexin variants are expressed (Schreiner et al., 2014; Treutlein et al., 2014). Adding to this complexity, the neurexin stalk region is modified by heparan sulfate (HS) in a subset of neurexins (Zhang et al., 2018).

Neurexins organize both the pre- and postsynaptic machinery and determine specific synaptic properties by forming trans-synaptic complexes with a multitude of diverse ligands that include intracellular, transmembrane, and secreted proteins (Südhof, 2017). However, known neurexin ligands seem to account for only a fraction of neurexin interactions, and identifying and validating novel neurexin ligands remain a challenge.

FAM19As (FAM19A1-A5, aka TAFA1-5), constitute a family of brain-enriched proteins that are differentially expressed across brain regions (Tom Tang et al., 2004; Yong et al., 2020; Fig. S1). FAM19As resemble cytokines and are evolutionarily highly conserved in vertebrates, but their functions remain enigmatic. FAM19As contain a signal peptide followed by a conserved region with 10 cysteine residues that likely form intramolecular disulfide bonds and include a CC-chemokine motif with distant homology to macrophage inflammatory protein 1α (Tom Tang et al., 2004).

Fam19a1 knockout (KO) mice have decreased body weights, are hyperactive, and exhibit reduced anxiety-like behaviors as well as impaired fear memory acquisition and recall (Lei et al., 2019; Yong et al., 2020). In contrast, *Fam19a2* and *Fam19a3* KO mice exhibit increased anxiety-like behaviors (Choi et al., 2018; Kim et al., 2017), while *Fam19a4* KO mice show increased injury-induced pain hypersensitivity and abnormal neuronal excitability (Delfini et al., 2013). These findings broadly suggest that FAM19As are important for normal nervous system function, but a mechanistic understanding of their roles is lacking. A number of potential receptors for FAM19As have been reported, including G-protein–coupled receptor 1 for FAM19A1 (Zheng et al., 2018), formyl-peptide receptor (FPR) 1 for FAM19A4 (Wang et al., 2014), and FPR2 and sphingosine-1-phosphate receptor 2 for FAM19A5 (Park et al., 2017; Wang et al., 2018). However, stoichiometric interactions were not documented for these putative receptors, and the FAM19A binding sites remain uncharacterized.

In the present study, we have identified FAM19A1-A4 proteins as stoichiometric subunits of neurexin complexes. We first detected FAM19A1 and FAM19A2 in a proteomic screen of endogenous neurexin complexes immuno-isolated from mouse brain. FAM19A1-A4 bind to all major neurexin isoforms by forming intermolecular disulfide bridges via the neurexin CysL-domain and via binding to an adjacent sequence of neurexins. Neurexins, in turn, are required for the stable expression and surface transport of FAM19A1. Exogenous FAM19A1 impairs neurexin *O*-glycosylation and HS modification, and lowers the levels of total, but not surface-localized, α-neurexins in mixed neuron/glia cultures obtained from mouse hippocampus. Thus, our findings deorphanize a family of brain-enriched putative cytokines as neurexin ligands and demonstrate that FAM19As regulate neurexin modifications, thereby expanding our understanding of the neurexin interactome to include regulatory subunits.

Results

Identification of FAM19A1-A4 as neurexin ligands

To systematically identify neurexin ligands, we performed affinity immuno-purifications of endogenous neurexin-1 from adult mouse brain. Using quantitative liquid chromatography-tandem mass spectrometry (Sterky et al., 2017), we found that FAM19A1 and FAM19A2 were coimmunoprecipitated with neurexins (Fig. 1 A). FAM19A1 and FAM19A2 (aka TAFA1 and TAFA2; Tom Tang et al., 2004) belong to a family of five cysteine-rich, vertebrate-specific, and evolutionarily conserved secreted brain proteins (Fig. 1 A and Fig. S1). Consistent with a sequence resemblance to cytokines, FAM19As were shown to bind to several G-protein–coupled receptors (GPCRs; Park et al., 2017; Wang et al., 2014, 2018; Zheng et al., 2018). Given these previous findings, the purification of endogenous neurexin/FAM19A complexes from brain was surprising. However, we isolated FAM19A1 and FAM19A2 in a complex with neurexins from brain homogenates in independent experiments using multiple neurexin antibodies, suggesting that FAM19As are robust constituents of neurexin complexes in brain.

FAM19A1-A5 are highly homologous (Fig. 1 A), suggesting that FAM19A3, FAM19A4, and FAM19A5 may also bind to neurexins. To test this and to validate the interactions of FAM19A1 and FAM19A2 with neurexins, we performed coimmunoprecipitation (coIP) experiments with recombinant proteins. We coexpressed in transfected HEK293T cells each of the five FAM19A isoforms (tagged with a C-terminal V5 epitope) and secreted, truncated neurexin-1β (Nrxn1β-ECD). Nrxn1β-ECD was tagged with a C-terminal Myc epitope and contained all Nrxn1β extracellular domains, but lacked its transmembrane region and cytoplasmic tail. We immunoprecipitated FAM19A1-A5 from the transfected HEK293T cell medium using V5 antibodies and analyzed the immunoprecipitates by immunoblotting for Nrxn1β and FAM19As (Fig. 1 B). We also examined a Nrxn1β mutant in which the CysL-domain of neurexins was deleted (referred to as Nrxn1β-ECD-ΔCysL) because we observed possible disulfide bonding of FAM19As with Nrxn1β (see below). The immunoprecipitations of secreted neurexin/FAM19A complexes revealed that FAM19A1-A4, but not FAM19A5, bound to the Nrxn1β-ECD (Fig. 1 B). Strikingly, deletion of the CysL-domain of Nrxn1β abolished FAM19A-binding.

FAM19A1-A4 form disulfide-bonded complexes with all neurexin splice variants tested

To independently confirm binding of FAM19As to Nrxn1β, we analyzed the medium of HEK293T cells coexpressing Nrxn1β-ECD or Nrxn1β-ECD-ΔCysL with FAM19A1-A5 by non-reducing or reducing SDS-PAGE and immunoblotting (Fig. 1 C). Under non-reducing conditions, Nrxn1β migrated as a covalent complex with FAM19A1-A4, but not with FAM19A5. The Nrxn1β/FAM19A complexes were absent after deletion of the CysL-domain and were dissociated by reducing agents (Fig. 1 C).

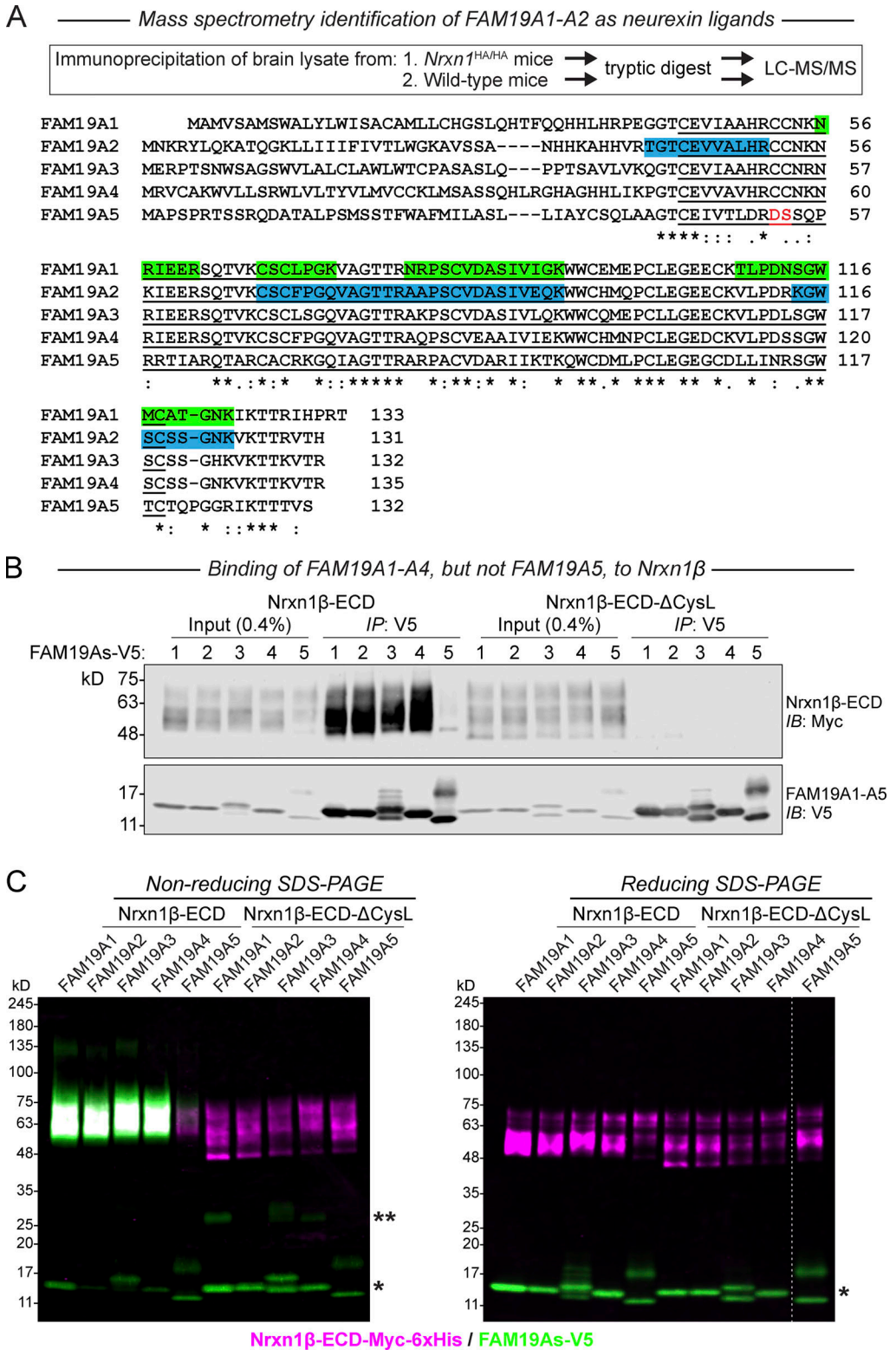

Figure 1. **Identification of FAM19A1-A4 as neurexin ligands. (A)** Identification of FAM19A1 and FAM19A2 as endogenous neurexin ligands. Top: Schematic of proteomic screen; bottom, alignment of *Mus musculus* FAM19A1-A5 amino acid sequences highlighting peptides identified by Mascot [FAM19A1, green; FAM19A2, blue; underline, TAFA domain ($CX_7CCX_{13}CXCX_{14}CX_{11}CX_4CX_5CX_{10}C$); asterisks, colons, and periods indicate fully, strongly, or weakly conserved residues, respectively; red, DS residues in FAM19A5 that replace conserved CC residues in FAM19A1-A4]. Neurexin complexes affinity purified from *Nrxn1*$^{HA/HA}$ or WT (negative control) adult mouse brains were analyzed by LC-MS/MS. **(B and C)** Recombinant FAM19A1-A4, but not FAM19A5, binds to Nrxn1β. FAM19As (FAM19A1-V5 to -A5-V5) were coexpressed in HEK293T cells with either secreted WT (Nrxn1β$^{SS4\text{-}SS5\text{-}}$-ECD-Myc-6xHis) or cysteine-loop deleted Nrxn1β-ECD (Nrxn1β$^{SS4\text{-}SS5\text{-}}$-ECD-ΔCysL-Myc-6xHis). Nrxn1β/FAM19A complexes in the medium were analyzed by immunoprecipitation and reducing SDS-PAGE (B) or directly by non-reducing and reducing SDS-PAGE and immunoblotting (C; magenta, Myc; green, V5; white, overlap). IB, immunoblot; IP, immunoprecipitation; **, FAM19A homodimers; *, FAM19A monomers. All experiments were independently performed at least three times.

Subtype-specific peptides for FAM19A3 and FAM19A4 were not detected by mass spectrometry in our original experiments, probably because FAM19A3 and FAM19A4 expression are very low in brain (Fig. S1; Saunders et al., 2018; Tasic et al., 2018; Tom Tang et al., 2004; Zeisel et al., 2018).

Do FAM19A1-A4 proteins bind to all neurexin isoforms? To address this question, we measured the surface exposure of neurexin/FAM19A complexes on HEK293T cells expressing full-length neurexins. In this assay, we coexpressed various EGFP-tagged full-length neurexin isoforms or control proteins with V5-tagged FAM19A1-A5 proteins and imaged cell-surface levels of FAM19A1-A5 by immunocytochemistry (Fig. 2 and Fig. S2). As a positive control, we used cerebellin-1 (Cbln1), a secreted neurexin ligand (Matsuda and Yuzaki, 2011; Uemura et al., 2010). As expected, Cbln1 was displayed at the cell surface when Nrxn1β containing splice site 4 (SS4) was coexpressed, but not when Nrxn1β lacking SS4 was coexpressed with Cbln1 (Fig. 2, A and B). As a negative control, we used leucine-rich repeat transmembrane protein 2 (LRRTM2) because FAM19As are not expected to bind to LRRTM2 (Fig. 2 C).

When we analyzed various splice variants of α- and β-neurexins and all five FAM19As (FAM19A1-A5), we found that all neurexin splice variants tested formed surface-exposed complexes with coexpressed FAM19A1-A4, but not with FAM19A5 (Fig. 2, D–P; and Fig. S2). Thus, consistent with the immunoprecipitation experiments, FAM19A1-A4, but not FAM19A5, bind to α- and β-neurexins independent of alternative splicing.

FAM19A1 forms a stable, stoichiometric complex with Nrxn1β

To obtain direct evidence for a stable complex of neurexins and FAM19A1-A4, we purified recombinant Nrxn1β-ECD, Nrxn1β-ECD/FAM19A1 complexes, and FAM19A1 from the medium of transfected HEK293S cells (which lack *N*-acetylglucosaminyltransferase I, GnTI$^-$). Nrxn1β-ECD was Myc- and 6xHis-tagged, and FAM19A1 was V5- or Twin-Strep-tagged (Fig. 3 and Fig. S3, H–P). An *O*-linked glycosylation-deficient Nrxn1β-ECD mutant in which all serines and threonines in the *O*-glycosylated stalk region were changed to glycines was used to reduce the heterogeneity of recombinant Nrxn1β-ECD (note that neurexin is poorly HS-modified in HEK293 cells; Zhang et al., 2018). Whereas FAM19A1 was efficiently secreted from HEK293S cells in a complex with Nrxn1β-ECD, low levels of secreted FAM19A1 were detected when FAM19A1 was expressed alone (Fig. S3, H–J), suggesting that FAM19A1 is poorly secreted in the absence of neurexins. Moreover, recombinant FAM19A1, when expressed without neurexins, partly formed disulfide-bonded dimers (Fig. S3, B and L). To enable the purification of sufficient quantities of recombinant FAM19A1 for biophysical studies, we replaced the endogenous signal peptide with that of Igκ and tagged FAM19A1 with a Twin-Strep moiety that allows efficient affinity purification but confers microheterogeneity to FAM19A1 (Fig. 3 F), likely because the bacterial Twin-Strep tag is *O*-glycosylated in eukaryotic cells.

We analyzed purified recombinant Nrxn1β-ECD, FAM19A1, and Nrxn1β-ECD/FAM19A1 complexes by size-exclusion chromatography coupled with multi-angle light scattering (SEC-MALS) to determine their absolute molar masses (Fig. 3, G and H). These experiments revealed that the Nrxn1β-ECD is a monomer and FAM19A1 is a mixture of monomers and dimers in solution, while Nrxn1β-ECD and FAM19A1 form a stoichiometric heterodimer (Fig. 3 I). Thus, Nrxn1β-ECD and FAM19A1 form a stable 1:1 complex.

The disulfide-bonded Nrxn1β/FAM19A1 complex is assembled in the secretory pathway

We observed a robust FAM19A cell-surface signal in the surface-exposure assay when FAM19As were coexpressed with Nrxn1β (Fig. 2, Fig. S2, and Fig. S3, E and F). Upon adding recombinant FAM19A1 to cells expressing Nrxn1β, however, we detected only weak FAM19A1 binding that was independent of the Nrxn1β CysL-domain, suggesting it is non-specific (Fig. S3, E and F). Moreover, whereas coexpressed FAM19A1 was disulfide-bonded to Nrxn1β (Fig. 1 C and Fig. 5 E), mixing of recombinant FAM19A1 and Nrxn1β-ECD purified separately failed to produce disulfide-bonded Nrxn1β/FAM19A1 complexes (Fig. S3 G). Together, these results suggest that FAM19As bind to neurexins by forming intermolecular disulfide bridges during transport through the secretory pathway.

To test whether recombinant Nrxn1β/FAM19A1 complexes are also disulfide bonded, we analyzed purified recombinant Nrxn1β-ECD/FAM19A1 complexes by SDS-PAGE in the absence and presence of reducing agents (Fig. 4 A). The complex was stable in SDS-sample buffer in the absence of reducing agents despite a high concentration of SDS, but was dissociated by disulfide bond reduction. Furthermore, on native PAGE (in which the migration of proteins is not strictly dependent on molar mass), the Nrxn1β-ECD/FAM19A1 complex was maintained in the absence of reducing agents, but disrupted by reducing agents (Fig. 4 B).

These experiments show that in the complex, Nrxn1β and FAM19A1 are disulfide-bonded to each other. Are the disulfide bonds between Nrxn1β and FAM19A1 produced physiologically within the secretory pathway, or do they form artifactually in the oxidizing environment of the medium after secretion and/or cell lysis (Johnston and Südhof, 1990)? The observations that separately purified FAM19A1 and Nrxn1β-ECD do not spontaneously form covalent disulfide-bonded complexes (Fig. S3 G) and that recombinant FAM19A1 fails to bind to surface-displayed Nrxn1β (Fig. S3, E and F) indicate that the disulfide-bonded Nrxn1β/FAM19A1 complex results from chaperoned interactions in the secretory pathway. To independently test this hypothesis, we expressed Nrxn1β-ECD and FAM19A1 either alone or in combination in HEK293T cells, collected the cells and the medium directly in SDS-sample buffer, and analyzed the samples without or with the addition of reducing agents by SDS-PAGE and immunoblotting (Fig. 4, C and D). The Nrxn1β-ECD/FAM19A1 complex was readily detectable as a single band on SDS-PAGE under non-reducing conditions both in the medium and the cells when the two proteins were coexpressed. Thus, the complex likely forms in cells before secretion and exposure to the extracellular milieu, suggesting it is assembled in the secretory pathway.

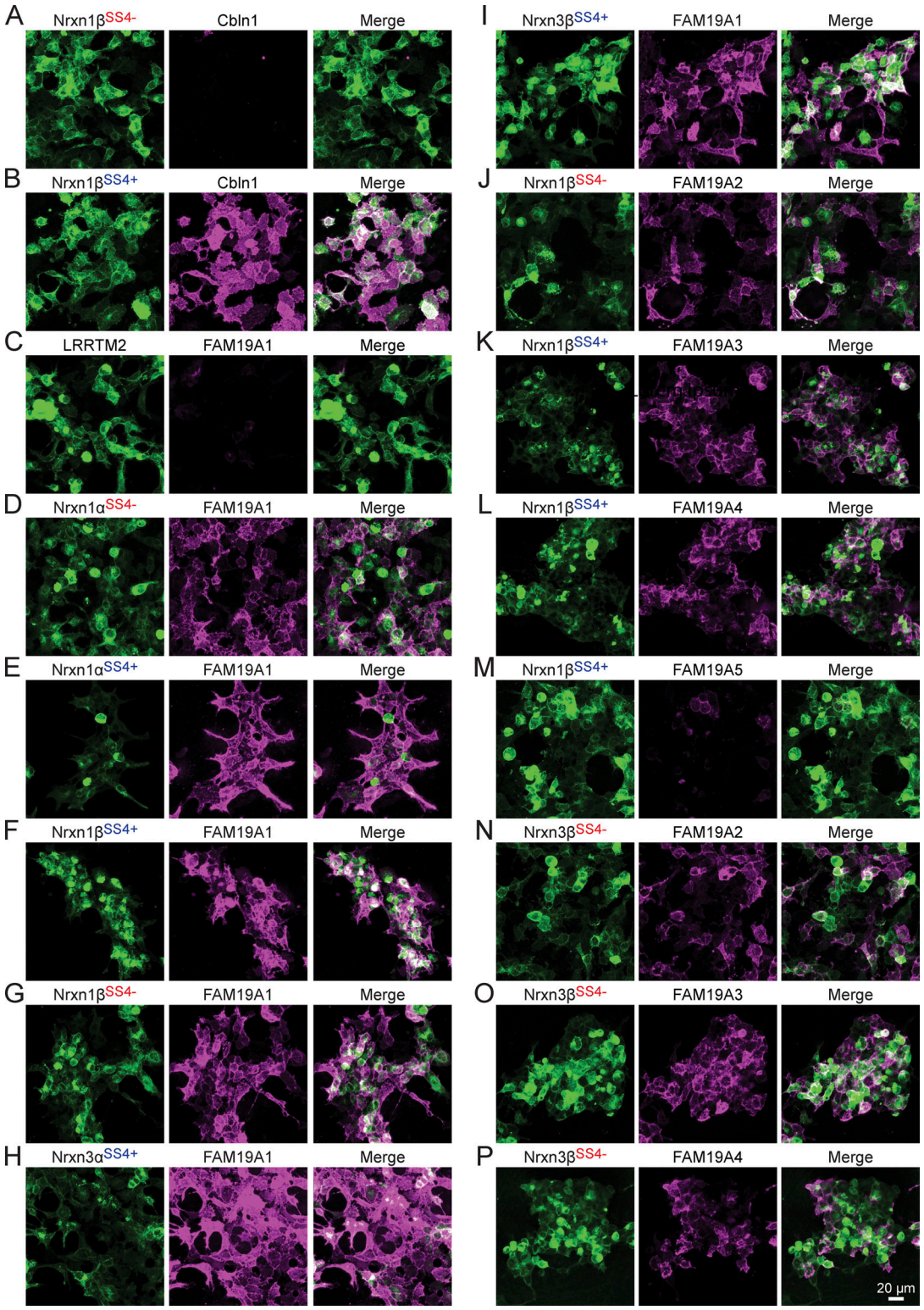

Figure 2. **All tested Nrxn1 and Nrxn3 isoforms form complexes with FAM19A1-A4, but not with FAM19A5, as visualized by imaging neurexin/FAM19A complexes on the surface of HEK293T cells coexpressing FAM19A and various neurexins. (A–P)** Representative images illustrating surface exposure of complexes formed by V5-tagged Cbln1 (A and B) or FAM19A1-A4 (C–P) with the indicated EGFP-tagged receptors in transfected HEK293T cells. Whereas Cbln1 only binds to the SS4$^+$ variant of Nrxn1, FAM19A1-A4 (but not FAM19A5) binds to SS4$^-$ and SS4$^+$ variants of Nrxn1 and Nrxn3, but not to LRRTM2 (negative control). Surface labeling was performed for V5 (magenta) and compared with the EGFP signal (green). For additional data, see Fig. S2 (n = 2–5 independent experiments).

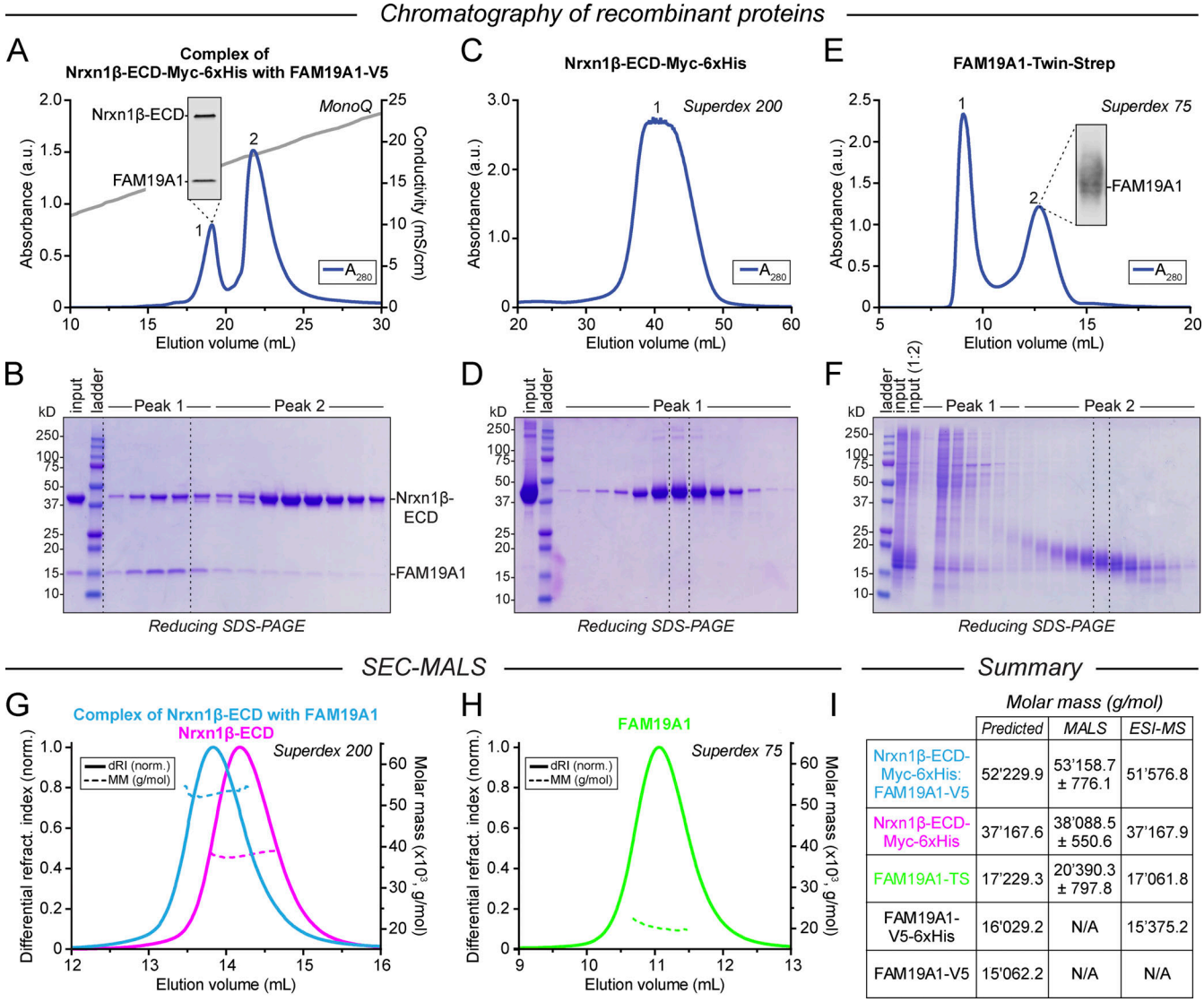

Figure 3. **Biophysical definition of the Nrxn1β/FAM19A1 complex. (A and B)** Nrxn1β-ECD (Nrxn1β-ECD-Myc-6xHis) was coexpressed with FAM19A1-V5 in HEK293S GnTI⁻ cells and purified from the medium. In the final purification step, the Nrxn1β-ECD/FAM19A1 complex elutes as a single peak (A, peak 1), as shown by Coomassie-blue staining (B) and immunoblotting for Myc and V5 (A, inset), whereas excess Nrxn1β-ECD elutes as a separate peak (A, peak 2). **(C and D)** Final purification step for Nrxn1β-ECD-Myc-6xHis, expressed alone, from the medium of HEK293S GnTI⁻ cells (C, elution profile; D, Coomassie-blue-stained reducing SDS-gel). **(E and F)** Final purification step for FAM19A1-Twin-Strep, expressed alone, from the medium of HEK293S GnTI⁻ cells (E, elution profile with Twin-Strep immunoblot in inset; F, Coomassie-blue-stained reducing SDS-gel). See also Fig. S3, H–P. **(G and H)** Nrxn1β-ECD forms a stoichiometric 1:1 complex with FAM19A1. Analysis by size-exclusion chromatography coupled with multi-angle light scattering (SEC-MALS) of the purified Nrxn1β-ECD/FAM19A1 complex and of Nrxn1β-ECD (G), and of FAM19A1 (H), which enables the determination of their precise molar masses (dRI, differential refractive index; MM, molar mass; dotted lines in B, D, and F denote fractions that were combined and analyzed). **(I)** Molar masses of the Nrxn1β-ECD/FAM19A1 complex, Nrxn1β-ECD, and FAM19A1 as predicted (Prot pi Protein Tool; assuming all cysteines form disulfide bonds and Nrxn1β contains one $Man_5GlcNAc_2$ addition) or as experimentally determined by MALS or electrospray ionization (ESI)-MS.

The cysteine residues of the Nrxn1β cysteine-loop domain are essential for the formation of covalent Nrxn1β/FAM19A1 complexes

We next investigated which neurexin sequences mediate the formation of the neurexin/FAM19A complex. Since all neurexin isoforms and splice variants tested form this complex (Fig. 2 and Fig. S2), we analyzed the FAM19A-binding sequences of Nrxn1β-ECD as the smallest neurexin variant that still binds to FAM19As. We systematically tested deletions of various Nrxn1β-ECD domains in Nrxn1β/FAM19A1 complex formation using coIPs (Fig. 5, A–D). Only the deletion of the CysL-domain of Nrxn1β blocked assembly of Nrxn1β/FAM19A1 complexes, although some Nrxn1β constructs were expressed poorly, likely due to misfolding (Fig. 5 B). In these experiments, we also examined whether *O*-glycosylation of the stalk domain of Nrxn1β is required for Nrxn1β/FAM19A1 complex formation, but observed no change in complex formation as a function of glycosylation (Fig. 5 B and Fig. S4 A).

The results from the deletion mutants agree with the original validation experiments of the neurexin/FAM19A complex, in

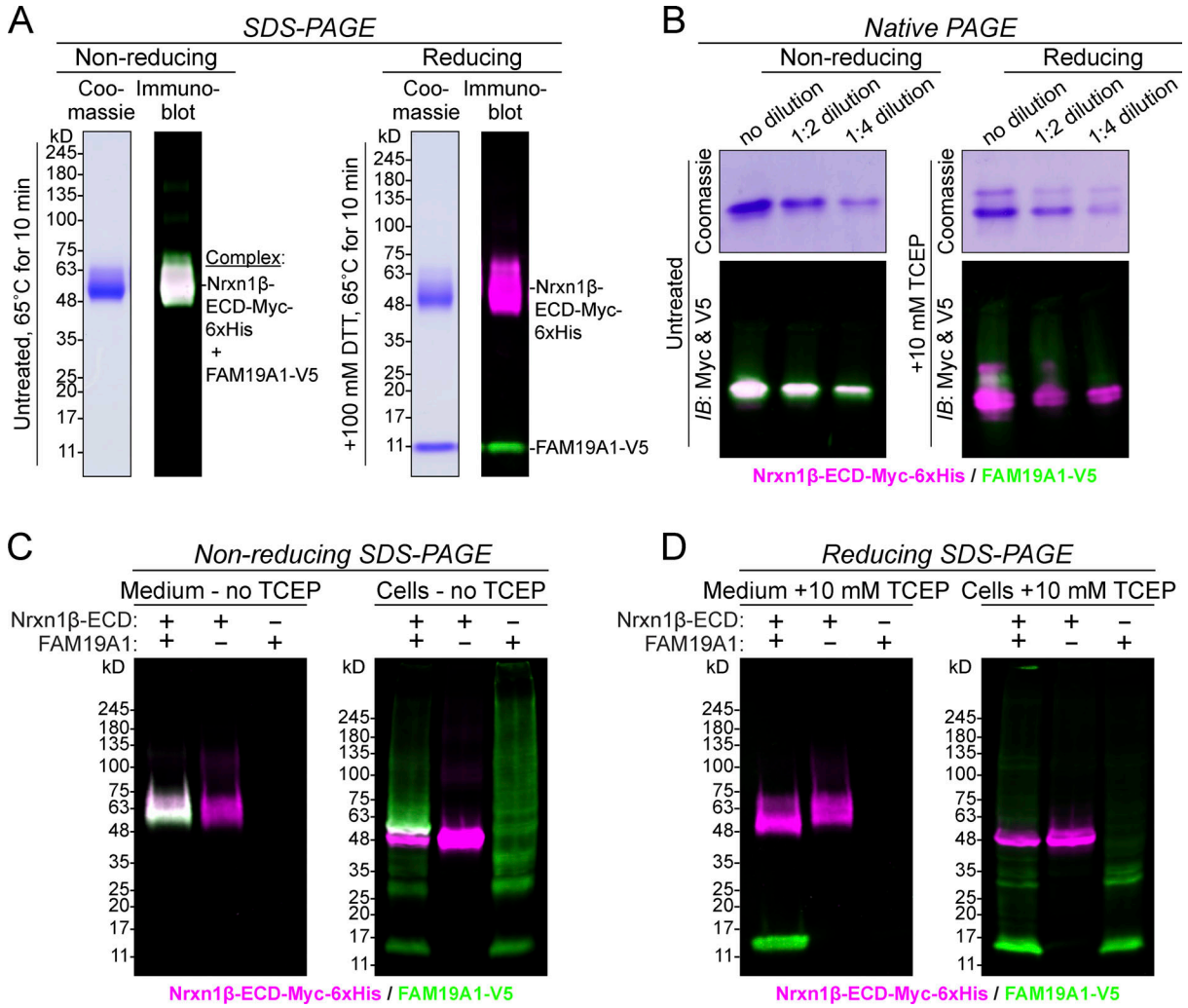

Figure 4. **The disulfide-bonded Nrxn1β-ECD/FAM19A1 complex is assembled in the secretory pathway. (A)** The purified recombinant Nrxn1β-ECD/FAM19A1 complex is dissociated by disulfide-bond reduction, but not by SDS-sample buffer alone (SDS-PAGE followed by Coomassie-blue staining or immunoblotting; magenta, Myc; green, V5; white, overlap; DTT, dithiothreitol). **(B)** The purified recombinant Nrxn1β/FAM19A1 complex is dissociated by disulfide-bond reduction also under native conditions (native PAGE followed by Coomassie-blue staining or immunoblotting; magenta, Myc; green, V5; white, overlap; TCEP, tris(2-carboxyethyl)phosphine). **(C and D)** The disulfide-bonded Nrxn1β/FAM19A1 complex is formed during intracellular transport of Nrxn1β and FAM19A1 in the secretory pathway. HEK293T cells coexpressing the indicated proteins and their media were separately collected in SDS-sample buffer and immunoblotted as indicated (magenta, Myc; green, V5; white, overlap). In the absence of Nrxn1β-ECD, FAM19A1 is largely retained as a disulfide-bonded aggregate in the cells. Cells expressing both the Nrxn1β-ECD and FAM19A1 in C contain Nrxn1β-ECD in a heterodimeric complex with FAM19A1 (white band) and as a monomer with a lower molecular weight (magenta band).

which deletion of the neurexin CysL-domain also blocked complex formation (Fig. 1, B and C). Since these findings suggest that the CysL-domain is essential for FAM19A binding, we analyzed its sequence in detail. The CysL-domain consists of a nine-residue loop with two flanking prolines and five negatively charged residues (CPSDDEDIDPC). Strikingly, no mutation of the loop sequence, including a substitution of positively charged arginines for the negatively charged residues, affected Nrxn1β/FAM19A1 complex formation (Fig. 5, C and D; and Fig. S4 A). Thus, despite remarkable sequence conservation, the actual sequence of the CysL-domain is not important for FAM19A1-A4 binding. Moreover, neither expanding the size of the loop by inserting two glycine residues nor replacing the entire nine-residue Nrxn1β CysL-domain with the non-homologous 13-residue cysteine-loop from Type A γ-aminobutyric acid $(GABA)_A$-β3 receptors (Miller and Aricescu, 2014) disrupted binding (Fig. 5, C–E). Mutation of the two cysteine residues forming the disulfide-bonded loop (Sterky et al., 2017), however, completely abolished formation of Nrxn1β/FAM19A1 complexes (Fig. 5, C–E). Thus, the only feature of the Nrxn1β CysL-domain that appears to enable FAM19A1 binding is the cysteine-loop itself, not its size or sequence.

These observations raised the question of whether FAM19A1 generally binds to all cysteine-loop domains. However, the extracellular domain of neuroligin-1 containing an insert in splice site A1 that includes disulfide-bonded loops (Araç et al., 2007; Hoffman et al., 2004; Ichtchenko et al., 1996) failed to form a complex with FAM19A1 (Fig. 5 D and Fig. S4 A), suggesting

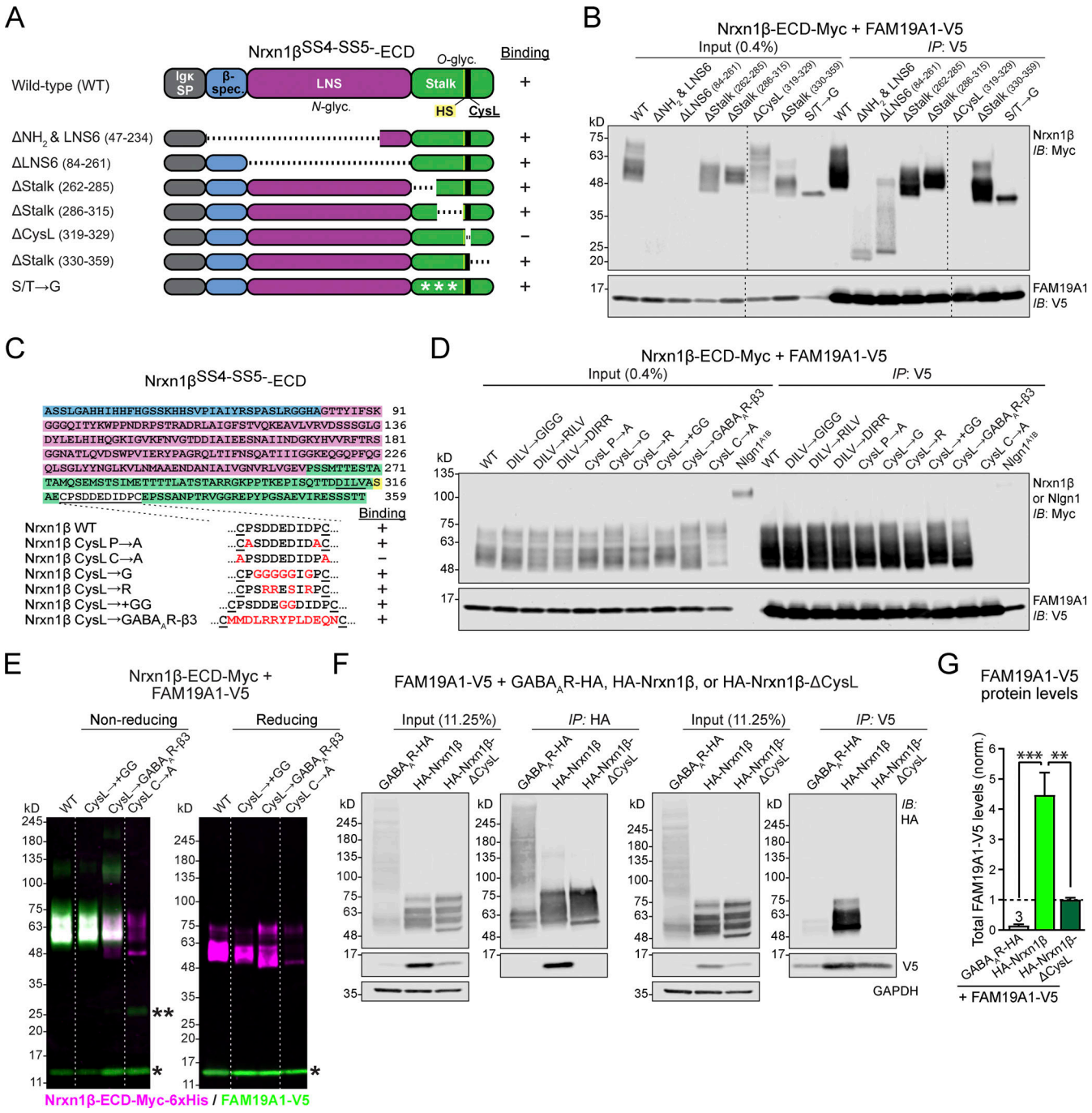

Figure 5. **FAM19A1 binding to Nrxn1β requires the cysteine-loop domain of Nrxn1β. (A)** Schematic of Nrxn1β constructs used for deletion mapping experiments (all on the Nrxn1β$^{SS4\text{-}SS5\text{-}}$-ECD backbone; Igκ SP, Igκ signal peptide; β-spec., β-Nrxn-specific sequence; LNS, sixth LNS domain [the only LNS-domain of β-neurexins]; stalk, *O*-glycosylated sequence separating the LNS-domain from the transmembrane region that is interrupted by the cysteine-loop (CysL) domain; *N*-glyc. and *O*-glyc., *N*- and *O*-linked glycosylation sites; HS, heparan sulfate modification site). **(B)** Coimmunoprecipitation (coIP) assays demonstrate that the CysL-domain of Nrxn1β is required for FAM19A1 binding. FAM19A1-V5 was coexpressed with wild-type (WT) or mutant Nrxn1β-ECDs (as Nrxn1β$^{SS4\text{-}SS5\text{-}}$-ECD-Myc-6xHis constructs) in HEK293T cells. FAM19A1 was immunoprecipitated from the medium using V5 antibodies and immunoblotted as indicated. **(C)** Amino acid sequences of the WT Nrxn1β-ECD (top) and of the various CysL-domain mutants analyzed for FAM19A1 binding (bottom). **(D)** coIPs performed as described for B demonstrate that, apart from the two cysteine residues, the CysL sequence of Nrxn1β is irrelevant for FAM19A1 binding, and that insertion of a cysteine-loop sequence from GABA$_A$R-β3 into the CysL of Nrxn1β does not impair FAM19A1 binding. Splice site A1-containing Nlgn1 was used as a negative control. **(E)** Immunoblotting analyses confirm that mutation of the Nrxn1β CysL-domain cysteines, but not of the actual loop itself, impairs FAM19A1 binding. The media of HEK293T cells coexpressing FAM19A1-V5 with WT or mutant Nrxn1β-ECDs were analyzed by SDS-PAGE under reducing and non-reducing conditions, followed by immunoblotting (magenta, Myc; green, V5; white, overlap). Disulfide-bonded FAM19A1 dimers are detected under non-reducing conditions when FAM19A1 is coexpressed with a non-binding Nrxn mutant (CysL→A). **, FAM19A1 homodimers; *, FAM19A1 monomers. See also Fig. S4 A. **(F)** coIP assays of HEK293T lysates coexpressing FAM19A1-V5 with the HA-tagged GABA$_A$R-β3, Nrxn1β, or mutant Nrxn1β lacking the CysL-domain show that GABA$_A$-β3 receptors do not bind to FAM19A1. **(G)** Quantifications of FAM19A1 protein levels in input fractions of experiments shown in F demonstrate that

Nrxn1β is required for high-level expression of FAM19A1. FAM19A1 protein levels were normalized to GAPDH and divided by coexpressed recombinant protein levels (i.e., $GABA_AR$-β3, Nrxn1β, or Nrxn1β-ΔCysL normalized to GAPDH), followed by normalization to the negative control group (Nrxn1β-ΔCysL). Data are means ± SEM, $n = 3$ experimental replicates. Statistical analyses were performed using a one-way ANOVA with Tukey's post hoc test for multiple comparisons (**, $P < 0.01$; ***, $P < 0.001$). Images depict representative blots from experiments that were independently replicated at least three times (B and D–G). IB, immunoblot; IP, immunoprecipitation.

specificity. To test this further, we asked whether FAM19A1 could form a complex with the solvent-exposed cysteine-loops of $GABA_A$-β3 receptors (Miller and Aricescu, 2014). We coexpressed FAM19A1-V5 with HA-tagged full-length Nrxn1β (positive control), mutant full-length Nrxn1β lacking the CysL-domain (negative control), and $GABA_A$-β3 receptors. We then measured binding of FAM19A1 to these proteins using coIPs with antibodies against HA or V5 (Fig. 5 F). FAM19A1 did not bind to $GABA_A$-β3 receptors, suggesting that the cysteine-loop domain alone cannot form neurexin/FAM19A complexes. Consistent with this conclusion, FAM19A1 did not bind to Nrxn1γ, which contains the CysL-domain of Nrxn1β but differs in its upstream sequences and which does bind to CA10, another recently described cis-ligand of neurexins (Fig. S4, B and C; Sterky et al., 2017).

We noted that whenever we coexpressed FAM19A1 with a protein that does not bind to FAM19A1, such as Nrxn1β lacking a CysL-domain or $GABA_A$-β3 receptors (Fig. 5 F), FAM19A1 levels appeared to be lower than when FAM19A1 was coexpressed with a neurexin that binds to FAM19A1, despite the fact that the expression conditions were the same. Quantifications confirmed that the secretion of FAM19A1 was ∼5- and ∼30-fold higher, respectively, when FAM19A1 was coexpressed with WT Nrxn1β than when it was coexpressed with mutant Nrxn1β or with $GABA_A$-β3 receptors (Fig. 5 G). These observations, consistent with the finding that FAM19A1 is poorly transported through the secretory pathway in the absence of neurexin (Fig. S3, H–J), support the conclusion that neurexin binding to FAM19A1 in the secretory pathway stabilizes FAM19A1.

FAM19A1 has no effect on synapse formation but alters inhibitory synaptic transmission

Since neurexins shape synapse properties (Südhof, 2017), does FAM19A1 binding to neurexins affect synapse formation and/or synaptic transmission? To address this question, we prepared mixed cultures of neurons and glia from the hippocampus of newborn mice that are triple homozygotes for the conditional knockout (cKO) of neurexins-1, -2, and -3 (referred to as Nrxn123 cKO mice; Chen et al., 2017). We infected the cultures at day in vitro (DIV) 4 with lentiviruses encoding mutant inactive (ΔCre; control; Kaeser et al., 2009) or active Cre-recombinase (Cre), and at DIV6 with lentiviruses encoding FAM19A1-V5 or with control lentiviruses. We analyzed the cultures by immunocytochemistry, biochemistry, and electrophysiology at DIV14–16. With this experimental design, we compared cultures expressing or lacking α- and β-neurexins, without or with coexpression of FAM19A1 (see Fig. S5, E and F, demonstrating that the Nrxn123 cKO ablates neurexin expression).

Immunocytochemical labeling for vesicular glutamate transporter 1 (vGluT1) and vesicular GABA transporter (vGAT), markers for excitatory and inhibitory synapses, respectively, showed that neither the neurexin deletion nor the expression of exogenous FAM19A1 had a significant effect on synaptic puncta density or size, quantified at secondary or tertiary dendrites visualized by MAP2 staining (Fig. 6, A–C and G–I). These results agree with previous studies demonstrating that neurexins are not essential for synapse formation (Chen et al., 2017; Luo et al., 2020; Missler et al., 2003) and suggest that FAM19A1 as a neurexin ligand is not required for synapse formation.

Next, we asked whether FAM19A1 regulates synaptic transmission even if it does not affect synapse numbers. To gain initial insight into this question, we measured miniature excitatory and inhibitory postsynaptic currents (mEPSCs and mIPSCs, respectively) as a function of exogenous FAM19A1 expression (Fig. 6, D–F and J–L). We observed only a modest effect of FAM19A1 on mEPSC amplitudes and frequencies (Fig. 6, D–F). However, FAM19A1 caused a significant decrease (∼20%) in mIPSC frequency (Fig. 6, J–L), suggesting that FAM19A1 binding to neurexins impacts synaptic function.

Neurexins are essential for the surface transport of FAM19A1

In the experiments of Fig. 6, we also analyzed surface-displayed FAM19A1 as a function of neurexin expression. FAM19A1 was abundantly present on the neuronal cell surface in a punctate pattern when endogenous neurexins were present (Fig. 6, A and G; and Fig. S5, A and B). Deletion of neurexins, however, decreased surface-displayed FAM19A1 levels dramatically (∼75–90%; Fig. 6 A, C, G, and I; and Fig. S5, A and B). FAM19A1 "puncta" were more abundant than synaptic puncta as identified by immunocytochemistry for vGluT1 and vGAT (Fig. 6), and were primarily localized at dendrites (Fig. S5, A and B). These results suggest that neurexins are the major binding partners of FAM19A1 because their deletion greatly decreases the levels of exogenously expressed surface-displayed FAM19A1.

FAM19A1 controls *O*-glycosylation and heparan sulfate (HS) modification of neurexins

Given that neurexins are essential for surface transport of FAM19A1, does FAM19A1 regulate the intracellular transport and post-translational modification of neurexins? To address this question, we generated dissociated hippocampal cultures containing or lacking endogenous α- and β-neurexins without or with expression of exogenous FAM19A1 as described in Fig. 6. We then biotinylated the cell-surface proteins of these cultures at DIV16, purified the biotinylated cell-surface proteins using streptavidin, and analyzed the total cellular proteins ("input"), "flowthrough" proteins (non-biotinylated, predominantly intracellular proteins), and "biotinylated" purified cell-surface proteins (Fig. 7 A).

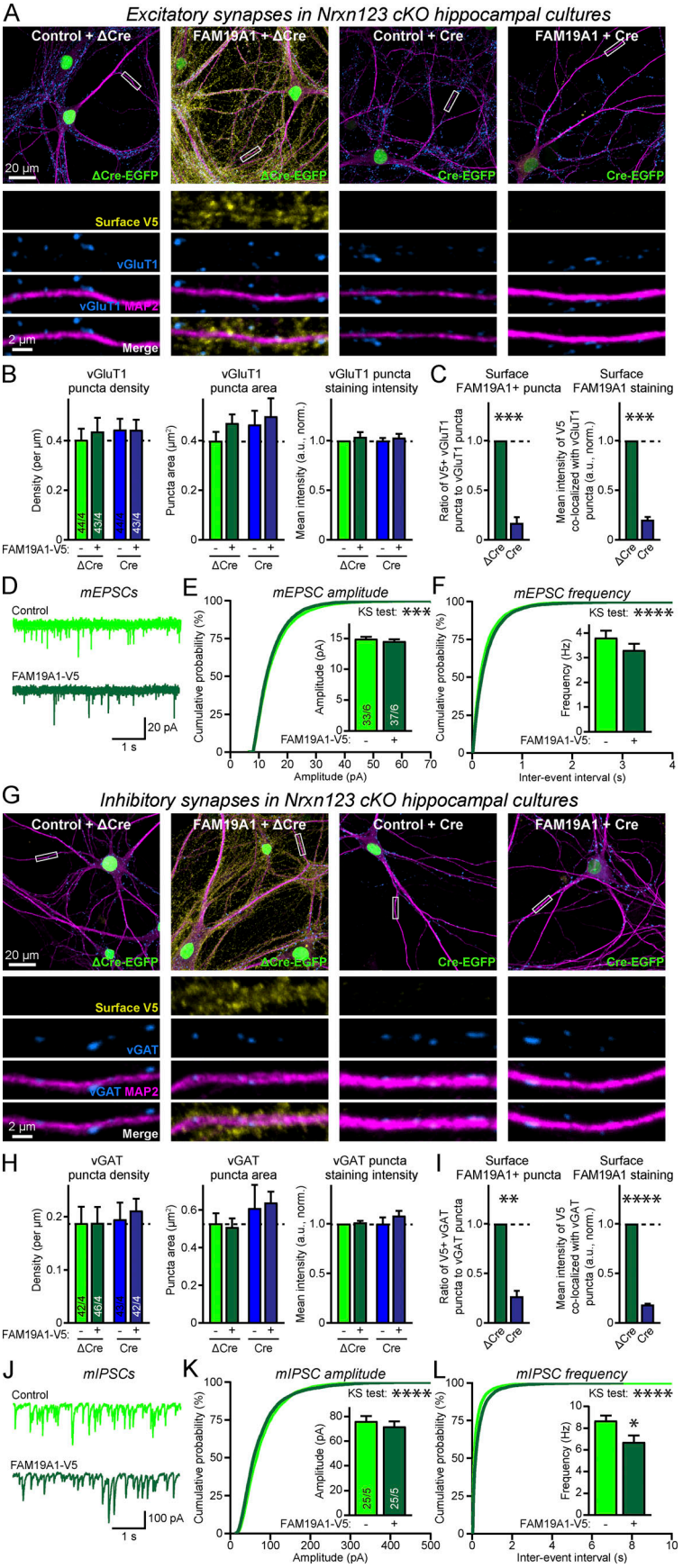

Figure 6. **Neurexins are essential for the surface transport of FAM19A1 in hippocampal neurons.** Hippocampal cultures from newborn Nrxn123 cKO mice were infected at DIV4 with lentiviruses encoding Cre or ΔCre, and at DIV6 with lentiviruses encoding FAM19A1-V5 or control lentiviruses. Analyses were performed at DIV14–16. **(A)** Representative images of neurons stained for surface-exposed FAM19A1-V5 (yellow) to monitor surface expression of FAM19A1 and for intracellular MAP2 (magenta) and vGluT1 (blue) to visualize excitatory synapses (top, overviews; bottom, expanded views of dendrites used for quantifications). Neuronal nuclei express EGFP-tagged Cre or ΔCre (green). **(B)** Expression of FAM19A1 and deletion of neurexins have no significant effect on excitatory synapse density, size, or staining intensity. **(C)** Deletion of neurexins nearly abolishes surface transport of FAM19A1. Left, ratio of vGluT1-positive synaptic puncta coincident with surface FAM19A1-V5. Right, surface FAM19A1-V5 staining mean intensity coincident with vGluT1-positive synaptic puncta. **(D–F)** Miniature excitatory postsynaptic current (mEPSC) recordings. Exogenous FAM19A1 has a modest effect on mEPSC amplitude (E) and frequency (F). **(G–I)** Same as A–C, except that inhibitory synapses labeled for vGAT were analyzed instead of excitatory synapses labeled for vGluT1. **(J–L)** Miniature inhibitory postsynaptic current (mIPSC) recordings. Exogenous FAM19A1 has no effect on mIPSC amplitude (K), but reduces mIPSC frequency (L). All numerical data are means ± SEM (n = 4 independent cultures for B, C, H, and I; n = 33–37 cells from six independent cultures for D–F; n = 25 cells from five independent cultures for J–L). Mean intensity values are normalized to the control group within each experimental replicate. Statistical analyses of puncta density and area (B and H) were performed using a two-way ANOVA (factors: FAM19A1-V5 +/–, ΔCre/Cre) with Tukey's post hoc test for multiple comparisons. Mean intensity data (B, C, H, and I) were analyzed using two-tailed one-sample t tests. Data in E, F, K, and L were analyzed using two-tailed unpaired t tests. Cumulative distributions were analyzed using Kolmogorov–Smirnov (KS) tests (*, P < 0.05; **, P < 0.01; ***, P < 0.001; ****, P < 0.0001).

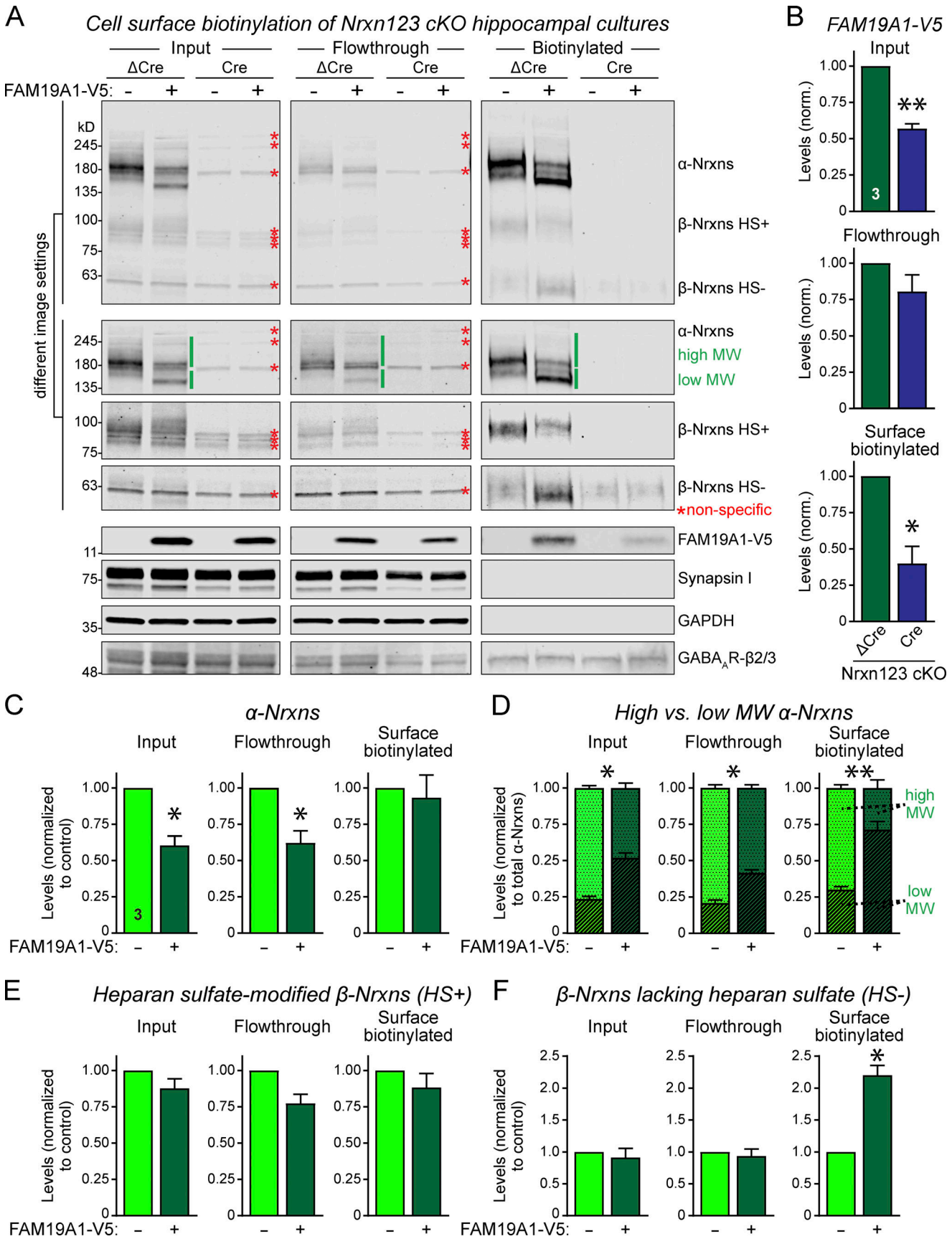

Figure 7. **FAM19A1 expression depends on neurexins and alters the levels and apparent size of α-neurexins. (A)** Representative immunoblots illustrating that Nrxns are required for stable FAM19A1 expression and that FAM19A1 expression changes the apparent size and levels of α-neurexins. Cell-surface

proteins of hippocampal cultures (prepared as described for Fig. 6) were biotinylated at DIV16 and purified using streptavidin. Input, flowthrough, and biotinylated fractions were analyzed by immunoblotting. Two exposures of the neurexin immunoblot are shown to illustrate various molecular weight species. Red asterisks, non-specific bands detected using the pan-neurexin antibody ABN161-I. **(B)** Deletion of all neurexins decreases total and surface, but not intracellular, FAM19A1 levels, demonstrating that neurexins enable surface-transport of FAM19A1. **(C)** FAM19A1 reduces total and intracellular, but not surface, α-neurexin levels. **(D)** FAM19A1 decreases the relative abundance of highly glycosylated "high molecular weight" α-neurexins and increases the relative abundance of less glycosylated "low molecular weight" α-neurexins in all fractions. **(E)** FAM19A1 has no effect on heparan sulfate (HS)-modified (HS^+) β-neurexin levels, identified as high molecular weight β-neurexin variants that disappear with the addition of heparinases (see Fig. 8). **(F)** FAM19A1 has no effect on total or intracellular, but increases surface, HS^- β-neurexin levels. Data in B–F are means ± SEM (n = 3 independent cultures with at least three biological samples pooled per condition). Data in B, C, E, and F are normalized to GAPDH and the control group within each experimental replicate. Data in D are normalized to total α-neurexin levels within each group. Statistical analyses were performed using two-tailed one-sample t tests (B, C, E, and F) or paired t tests (D; *, $P < 0.05$; **, $P < 0.01$).

We first reexamined the effects of endogenous neurexins on exogenous FAM19A1. Deletion of neurexins suppressed total (~45% decrease) and surface-exposed FAM19A1 levels (~60% decrease, Fig. 7 B), confirming the conclusion of Fig. 6 that neurexins are the major physiological binding partners of FAM19A1 and suggesting that neurexin sequences within or surrounding the CysL-domain are not saturated by endogenous ligands.

Next, we examined the effects of exogenous FAM19A1 on neurexins. Surprisingly, exogenous FAM19A1 expression decreased (~40%) the total levels of α-neurexins without changing their surface levels (Fig. 7 C). Furthermore, FAM19A1 caused a large shift in the apparent mobility of α-neurexins on reducing SDS-gels (Fig. 7 D). As shown below, this mobility shift was due to a FAM19A1-induced decrease in the *O*-glycosylation and HS modification of α-neurexins. Under control conditions, ~70% of surface α-neurexins were extensively *O*-glycosylated and/or HS-modified. Upon coexpression of FAM19A1, only ~30% of surface α-neurexins were extensively *O*-glycosylated and/or HS-modified (Fig. 7 D). Additionally, exogenous FAM19A1 increased the surface levels of non-HS–modified β-neurexins, although monitoring β-neurexins is difficult due to their low abundance and extensive glycosylation (Fig. 7, E and F).

To further characterize the effect of FAM19A1 on neurexins, we examined their *O*-glycosylation and HS modification in detail. We purified the biotinylated cell-surface proteins of cultured hippocampal cells without and with exogenous FAM19A1 expression as described above, and treated the surface proteins with a mix of glycosidases to remove *N*- and most *O*-linked sugars, or with heparinases I, II, and III to remove HS (Fig. 8 and Fig. S5 H). Afterward, we analyzed the proteins by reducing SDS-PAGE and immunoblotting.

As observed above (Fig. 7), exogenous FAM19A1 decreased the apparent molecular weight of most α- and β-neurexin bands by at least 20 kD (Fig. 8, B and E). Strikingly, *N*- and *O*-linked deglycosylation of neurexins caused a similar, but not identical, shift in apparent molecular weight of α-neurexins as exogenous FAM19A1 expression. The combination of FAM19A1 expression and deglycosylation, conversely, produced a slightly bigger shift in molecular weight than deglycosylation or FAM19A1 expression alone (Fig. 8, A–C). Whereas exogenous FAM19A1 had no detectable effect on HS-modified β-neurexins, it slightly decreased the apparent molecular weight of non-HS–modified β-neurexins. Viewed together, these results indicate that FAM19A1 significantly down-regulates neurexin *O*-glycosylation.

Heparinases also caused major shifts in the apparent molecular weights of neurexins, as shown previously (Zhang et al., 2018). These shifts differed from those observed for *N*- and *O*-deglycosylation, although for α-neurexins they were again broadly similar to shifts induced by exogenous FAM19A1 (Fig. 8, D–F). The combination of heparinases and FAM19A1 expression produced only a slightly bigger shift in the molecular weight of α-neurexins than either condition alone, suggesting that FAM19A1 suppresses the HS modification of neurexins (Fig. 8, E and F). Although heparinase treatment led to a similar de-enrichment of HS-modified β-neurexins with and without exogenous FAM19A1, a slight enrichment in lower molecular weight species was maintained with exogenous FAM19A1, which may be partly due to differences in *O*-glycosylation. Moreover, an analysis of surface proteins modified by HS using an antibody to the "HS stub," which remains on proteins after HS removal by heparinases, revealed that α-neurexins represent a minor component of the HS-modified proteome (Fig. S5 H).

Viewed together, these experiments suggest that subsets of α- and β-neurexins are modified by *O*-linked sugars and/or by HS. FAM19A1 appears to regulate both modifications. Given that in neurexins, both the serine that is modified by HS (Ser^{316} in Fig. 5 C; Zhang et al., 2018) and the serines and threonines that are *O*-glycosylated (Ushkaryov et al., 1992, 1994) are proximal to the FAM19A1 binding site and that FAM19A1 binding occurs within the secretory pathway, the regulation of these modifications by FAM19A1 is plausible.

Expression of FAM19As is activity-dependent in hippocampal cultures

The regulation of the *O*-glycosylation and HS modification of neurexins by FAM19As raises the question of whether such regulation is, in turn, regulated. As an initial approach to this question, we analyzed the expression of FAM19As and neurexins as a function of activity in hippocampal cultures (Fig. 9). Strikingly, neuronal depolarization decreased *Fam19a1* and *Fam19a2* expression by ~60% and ~20%, respectively, over a 48-h time course (Fig. 9, C and D). In contrast, *Car10* and *Nrxn3* were up-regulated ~30–40%, whereas *Car11* and *Nrxn2* were down-regulated ~25–30% (Fig. 9, F, G, I, and J). Since *Fam19a1*, *Fam19a2*, *Car10*, and *Car11* are differentially expressed in hippocampal neurons (Fig. S1, E–H), these data suggest that the expression of these genes is subject to divergent activity-dependent regulation.

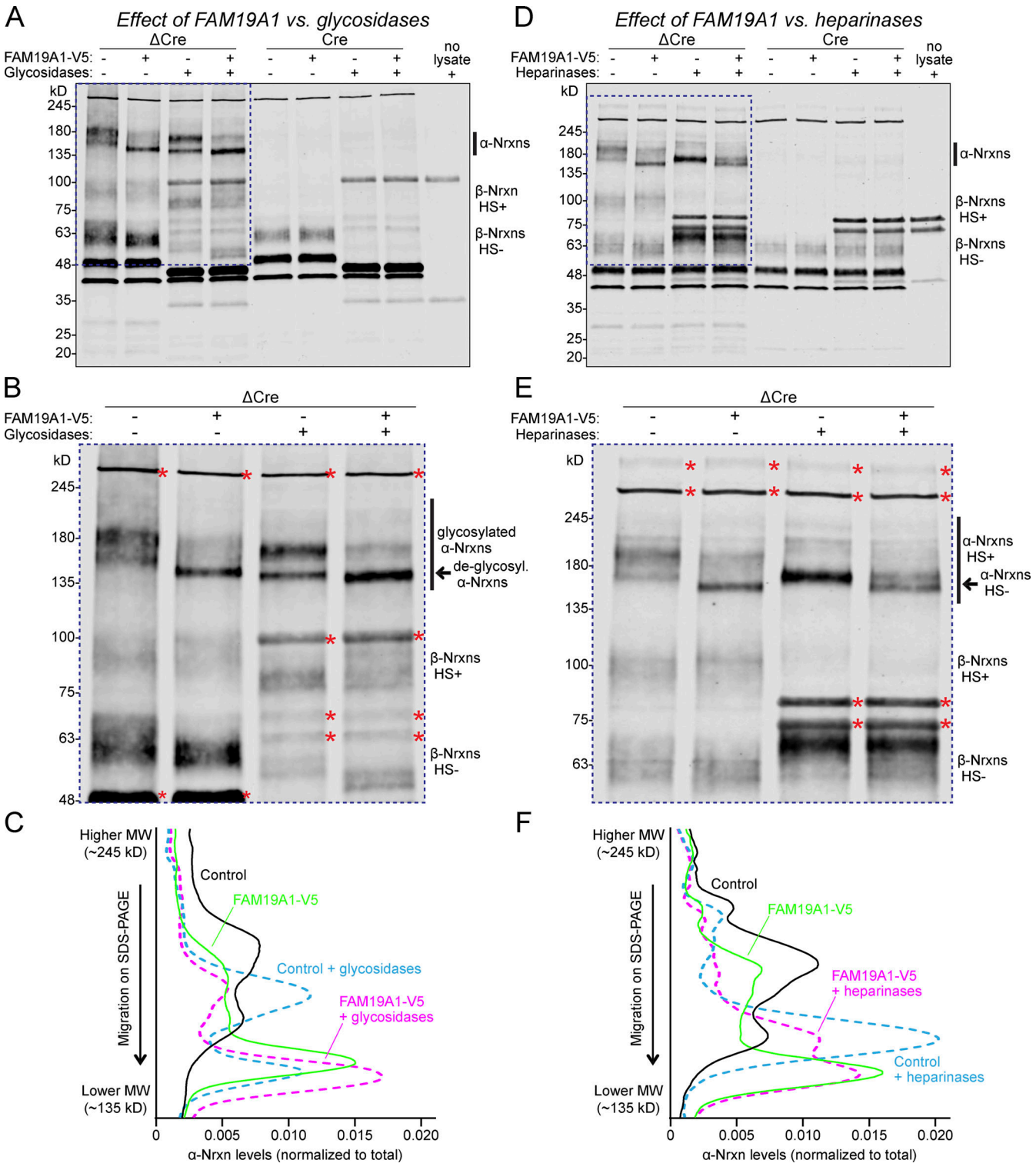

Figure 8. **FAM19A1 expression in hippocampal cultures suppresses the modification of cell-surface neurexins by *O*-glycans and heparan sulfate (HS).** Cell surface proteins in hippocampal cultures were biotinylated at DIV16 and purified using streptavidin before enzymatic treatment in the presence of reducing agents to prevent steric hinderance by neurexin stalk-binding ligands. Non-specific bands (red asterisks) detected by the pan-neurexin antibody were identified by their presence in immunoblots of Cre+ Nrxn123 cKO samples or enzymatic additions alone ("no lysate"). **(A–C)** Enzymatic removal of *N*- and *O*-linked glycans causes a major shift in the molecular weight (MW) of α-neurexins that resembles the shift in molecular weight observed by FAM19A1 expression, while β-neurexins exhibit a much smaller shift in molecular weight that is parallel to that induced by FAM19A1 expression. **(B)** Enlargement of the boxed area in A to illuminate band shifts. **(C)** Plot of the molecular weight distribution of α-neurexin signals indicated by the black line in A and B. **(D–F)** Enzymatic removal of HS modifications also causes a major shift in the molecular weight of α-neurexins that again resembles the shift in molecular weight observed by FAM19A1 expression, while β-neurexins are collapsed into more intense, smaller molecular weight species that are subtly influenced by FAM19A1 expression. HS modifications were removed using heparinases I, II, and III. Panel F contains a plot of the molecular weight distribution of α-neurexin signals indicated by the black line in D and E. Representative blots from at least three independent cultures, with at least three biological samples pooled per condition.

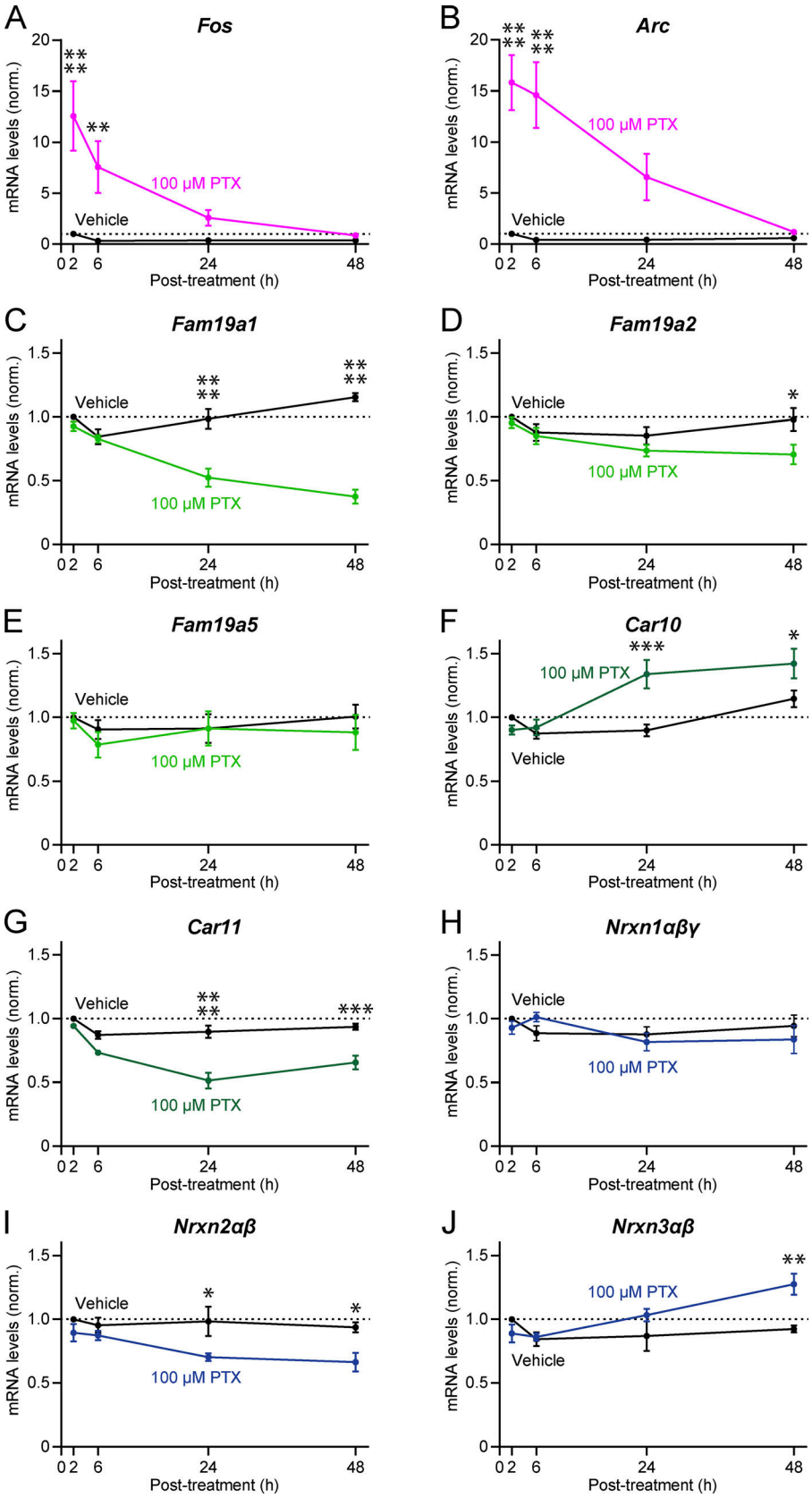

Figure 9. ***Fam19a1* transcript levels are activity-dependent. (A–J)** Hippocampal cultures generated from WT mice were treated at DIV14 with a $GABA_A$ receptor antagonist (100 µM picrotoxin [PTX], to increase neuronal activity) or vehicle. The mRNA levels of the indicated genes were analyzed by quantitative RT-PCR at 2, 6, 24, and 48 h post-treatment. Data are means ± SEM, normalized to the vehicle group 2 h post-treatment. *n* = 3–6 independent cultures, with 2–4 biological samples pooled per condition. Statistical analyses were performed using a repeated-measures two-way ANOVA with Tukey's post hoc test for multiple comparisons (*, P < 0.05; **, P < 0.01; ***, P < 0.001; ****, P < 0.0001).

Discussion

Neurexins are presynaptic adhesion molecules that function as central regulators of synapse properties (reviewed in Kasem et al., 2018; Südhof, 2017). Despite much work, however, the functions of neurexins and their mechanisms of action are incompletely understood. A major emerging theme for understanding neurexins is their vast number of physiological ligands, which at present encompass at least eight gene families (cerebellins, α-dystroglycan, neurexophilins, neuroligins, LRRTMs, calsyntenins, C1qls, and CA10/11) with more than 25 members. All of these ligands, except for CA10/11 (Sterky et al., 2017) and C1ql2/3 (Matsuda et al., 2016), bind to either the LNS2 or LNS6 domain, and for many domains of neurexins, no ligands have yet been described. Here, we identified FAM19A1-A4 as novel interactors of α- and β-neurexins that exhibit remarkable properties unlike other previously studied ligands. FAM19A1-A4 were presumed to be secreted cytokines that bind to GPCRs in a signaling function. However, we demonstrate that they are stoichiometric subunits of neurexin complexes. FAM19As are poorly secreted on their own and require neurexins for stable transport through the secretory pathway. All previously described ligands interact with neurexins in a reversible fashion, whereas the neurexin-binding mode of FAM19A1-A4 is unusual in that it requires transit through the secretory pathway and involves the formation of intermolecular disulfide bonds mediated by the neurexin CysL-domain. To the best of our knowledge, this is a structurally unprecedented interaction mode that differs from that of other neurexin ligands.

Seven lines of evidence demonstrate that the neurexin/FAM19A complex represents a physiological interaction, that neurexins are the predominant binding partners for FAM19A1-A4, and that their interaction serves to regulate post-translational processing of neurexins. First, well-controlled immunoprecipitations of endogenous neurexins from mouse brain showed that endogenous FAM19A1 and FAM19A2 are present in a complex with neurexins in brain (Fig. 1 A). Given that FAM19A isoforms are selectively expressed in small subsets of neurons throughout the brain (Fig. S1) and thus are not abundant proteins, and given the cis requirement for neurexin/FAM19A binding (Fig. S3, E–G), the robust detection of FAM19A1 and FAM19A2 in these immunoprecipitations suggests that neurexin/FAM19A complexes are prevalent in neurons expressing FAM19A1-A4 isoforms. Second, recombinant neurexins bind to FAM19A1-A4, but not FAM19A5, when produced in transfected HEK293T cells, as documented by coIPs, migration on SDS-PAGE under non-reducing but not reducing conditions, and surface exposure assays of FAM19A1-A4 and neurexins (Fig. 1, Fig. 2, and Fig. S2). Third, biophysical measurements, in particular SEC-MALS, demonstrated that Nrxn1β forms a stoichiometric, heterodimeric, covalent complex with FAM19A1 (Fig. 3 and Fig. 4). Fourth, mutagenesis showed that the two cysteine residues of the Nrxn1β CysL-domain were the only absolute requirement for assembly of the covalent Nrxn1β/FAM19A1 complex (Fig. 5). These two cysteine residues presumably bind to cysteine residues in FAM19A1-A4, which would explain why FAM19A5 does not bind because it lacks two conserved cysteine residues (Fig. 1 A). Additionally, the stoichiometry of the Nrxn1β/FAM19A1 complex suggests that it involves two intermolecular disulfide bonds. FAM19A1 binding to Nrxn1β was independent of the neurexin CysL sequence, but was specific overall since the cysteine-loop sequence of $GABA_A$-β3 receptors bound to FAM19A1 when it was transferred into Nrxn1β, but not when it was retained within $GABA_A$-β3 receptors. Moreover, Nrxn1γ, which contains the neurexin-1 CysL-domain and binds to CA10/11 but lacks other N-terminal neurexin-1 sequences (Sterky et al., 2017), did not bind to FAM19A1 (Fig. S4, B and C). Thus, additional N-terminal Nrxn1β sequences likely facilitate FAM19A binding even though no single specific sequence we tested was absolutely required. These data on the structure of the neurexin/FAM19A complex reveal a remarkable mechanism, namely the formation of a covalent complex in the secretory pathway. Fifth, FAM19A1 expression levels were significantly lower when FAM19A1 was expressed alone or coexpressed with non-binding proteins compared with when FAM19A1 was coexpressed with neurexins (Fig. 5, D, F, and G; and Fig. S4 A). Similarly, FAM19A1 expression levels were dramatically lowered when endogenous neurexins were deleted (Fig. 7 B), demonstrating that FAM19A1 requires neurexin binding for stability. Sixth, exogenously expressed FAM19A1 was displayed on the neuronal cell surface in a punctate pattern when endogenous neurexins were present, but was largely absent when endogenous neurexins were deleted (Fig. 6, C and I; and Fig. S5, A and B). Thus, neurexins are the major receptors for FAM19A1. Seventh and finally, FAM19A1 expression altered neurexin *O*-glycosylation and HS modification (Fig. 7, Fig. 8, and Fig. S5 H). Thus, consistent with a disulfide-mediated interaction that occurs within the secretory pathway, FAM19A1 regulates the post-translational modification of neurexins.

Viewed together, our results demonstrate that FAM19A1-A4 are physiological subunits of neurexin-ligand complexes. How can we reconcile our observations with studies suggesting that FAM19A1 and FAM19A4 are secreted ligands for G-protein–coupled receptor 1 (Zheng et al., 2018) and FPR1 (Wang et al., 2014), respectively? Our results do not rule out the possibility that FAM19As perform multiple functions and act as cytokines in non-neuronal cells and as subunits of neurexin complexes in neurons. However, all studies identifying putative receptors for FAM19As as candidate cytokines were performed by measuring surface binding of recombinant proteins to transfected cells. Although informative, such surface binding can be misleading given the small amounts of proteins involved and the indirect nature of the assay. No direct interaction studies with recombinant proteins, as shown in Fig. 3 here, were performed. Clarification of the role of the GPCRs implicated as FAM19A receptors will require such studies. It is remarkable that all GPCRs proposed as FAM19A receptors are also known to function as receptors for other unrelated ligands, and that different receptors were suggested for different FAM19A isoforms despite their homology.

What is the physiological role of the neurexin/FAM19A complex? Despite more than 1,000 papers, the functions of neurexins are only partly understood. A synaptic role is overwhelmingly demonstrated, but owing to the expression of thousands of splice variants, such a role appears to

be multifaceted and diverse (Südhof, 2017). In cultured neurons, neurexins have modest effects on synapses (see, for example, the lack of an effect of pan-neurexin deletions on synapse numbers in Fig. 6). However, in vivo neurexins control fundamental features of synapses, such as the release probability (Chen et al., 2017), Ca^{2+}-channels (Missler et al., 2003; Brockhaus et al., 2018; Luo et al., 2020), and post-synaptic receptor composition (Aoto et al., 2013; Dai et al., 2019). At synapses, neurexins form nanoclusters (Trotter et al., 2019), and the neurexin modifications that are regulated by FAM19As may affect such nanoclusters. *Fam19a* mRNAs are expressed in specific subsets of neurons throughout the brain (Saunders et al., 2018; Tasic et al., 2018; Zeisel et al., 2018; Fig. S1, E and F), which may give rise to the different phenotypes of *Fam19a1-a4* KO mice and add to the diversity of neurexin functions by conferring specific properties onto neurexins in neurons co-expressing FAM19As with neurexins. Consistent with this possibility, FAM19A1 regulates the diverse *O*-glycosylation and HS modification of neurexins, suggesting that FAM19As may shape the functional diversity of neurexins by controlling their post-translational modifications (Fig. 10). These modifications appear to affect the steady-state levels of neurexins, as shown by the decreased levels of total α-neurexins upon exogenous expression of FAM19A1 (Fig. 7 C), but more importantly likely alter ligand interactions of neurexins (Roppongi et al., 2020; Zhang et al., 2018). Consistent with a role for FAM19As in regulating neurexins, FAM19A1 is itself regulated by activity, as shown in a subset of excitatory neurons in vivo (Hrvatin et al., 2018) and as we observed in cultured hippocampal cells (Fig. 9). Such activity-dependent regulation of FAM19A expression in turn could contribute to the control of neurexin *O*-glycosylation and HS modification. Thus, we propose that FAM19As are selectively expressed in an activity-dependent manner in a subset of neurons to form stoichiometric cis-complexes with neurexins, thereby regulating their post-translational modifications and activities.

Materials and methods

Mice

Mice were group-housed with littermates of the same sex and maintained on a 12-h light/dark cycle, with access to food and water ad libitum. All procedures were performed in adherence with the National Institutes of Health Guide for the Care and Use of Laboratory Animals and were approved by the Stanford University Administrative Panel on Laboratory Animal Care.

Proteomic screen for endogenous neurexin ligands

The proteomic screen for endogenous neurexin ligands was previously described in Sterky et al. (2017). Briefly, brains from adult *Nrxn1*$^{HA/HA}$ (Trotter et al., 2019) or WT (negative control) mice were extracted and flash-frozen in the Südhof laboratory at Stanford University and sent to the Fakler laboratory at the University of Freiburg, where plasma membrane–enriched fractions were prepared. After solubilization with CL-91 buffer (Logopharm), membranes were subjected to affinity purification (AP; detailed in Schwenk et al., 2014) using the following antibodies: (1) anti-HA (Roche, 11867423001, lot 10145700), (2) anti-HA (Thermo Fisher Scientific, 26183, lot OJ187900), (3) anti-Nrxn1 (Synaptic Systems, 175103), or (4) anti-Nrxn2 (Südhof laboratory). Eluates of APs were trypsinized and analyzed by HPLC-coupled mass spectrometry (MS) using an Orbitrap Elite mass spectrometer (Thermo Fisher Scientific; as described in Schwenk et al., 2014). Protein amounts were quantified by a label-free procedure using peptide peak signal intensities (peak volumes, PV), and molecular abundances were estimated using the $abundance_{norm,\ spec}$ score, defined as the sum of all assigned and protein isoform-specific PVs divided by the number of MS-accessible protein isoform-specific amino acids (Bildl et al., 2012). The specificity of proteins copurified in APs was evaluated by calculating protein ratios (rPVs) from the respective peptide PVs (TopCorr method; Bildl et al., 2012). Specificity thresholds of APs were determined empirically from rPV histograms of all proteins detected in the respective AP versus control (samples from WT mice for anti-HA APs and from pre-immunization IgGs for anti-Nrxn APs). All proteins with rPVs above threshold in both anti-HA APs and at least one anti-Nrxn AP were considered specifically copurified.

Constructs

Unless otherwise noted, mouse protein coding sequences were used to generate all constructs. For transfections of HEK293T cells, constructs encoding FAM19A1-A5 or CA10 (Sterky et al., 2017) contained the endogenous signal peptide and were cloned into pEB-Multi-Neo (Fig. 1, B and C; Fig. 2; Fig. S2; Fig. S3, A–G; Fig. 4, A, C, and D; and Fig. S4; and Fig. 5). For transduction using BacMam viruses, the endogenous signal peptide was used for FAM19A1-V5 and FAM19A1-V5-6xHis (Fig. 3, A, B, G, and I; Fig. 4 B; and Fig. S3, H–J). For the BacMam virus encoding FAM19A1-Twin-Strep, the signal peptide was replaced with that of Igκ (Fig. 3, E, F, H, and I; and Fig. S3, K–O). For transfections of HEK293T cells, constructs encoding the WT or mutant Nrxn1β$^{SS4\text{-}SS5}$-ECD contained the Igκ signal peptide and were cloned into pEB-Multi-Neo (Fig. 1, B and C; Fig. 4, A, C, and D; Fig. 5, A–E; and Fig. S4 A). Similarly, BacMam virus encoding Igκ-Nrxn1β$^{SS4\text{-}SS5}$-ECD-ΔCHO-Myc-6xHis was used (Fig. 3, A–D, G, and I; Fig. 4 B; and Fig. S3 G; Sterky et al., 2017). For constructs encoding full-length neurexins with C-terminal EGFP tags, the endogenous signal peptides were used (Sterky et al., 2017; Fig. 2 and Fig. S2). For constructs in the HIV-1 flap, ubiquitin promoter, woodchuck hepatitis virus post-transcriptional regulatory element (FUW) vector encoding full-length WT or mutant Nrxn1β or Nrxn1γ with an HA tag downstream of the signal peptide, the endogenous signal peptide was used (Fig. 5, F and G; Fig. S3, E–F; and Fig. S4, B and C). $GABA_AR$-β3 was cloned into pCMV-Sport6 and contained a C-terminal HA tag, and the endogenous signal peptide was replaced with that of chicken LAR-type receptor phosphotyrosine-phosphatase σ (PTPRS; Miller and Aricescu, 2014; Fig. 5, F and G).

Cell culture

Hippocampal cultures

Hippocampal cultures containing neurons and glia (i.e., mixed) were generated from post-natal day (P) 0 Nrxn123 cKO mice

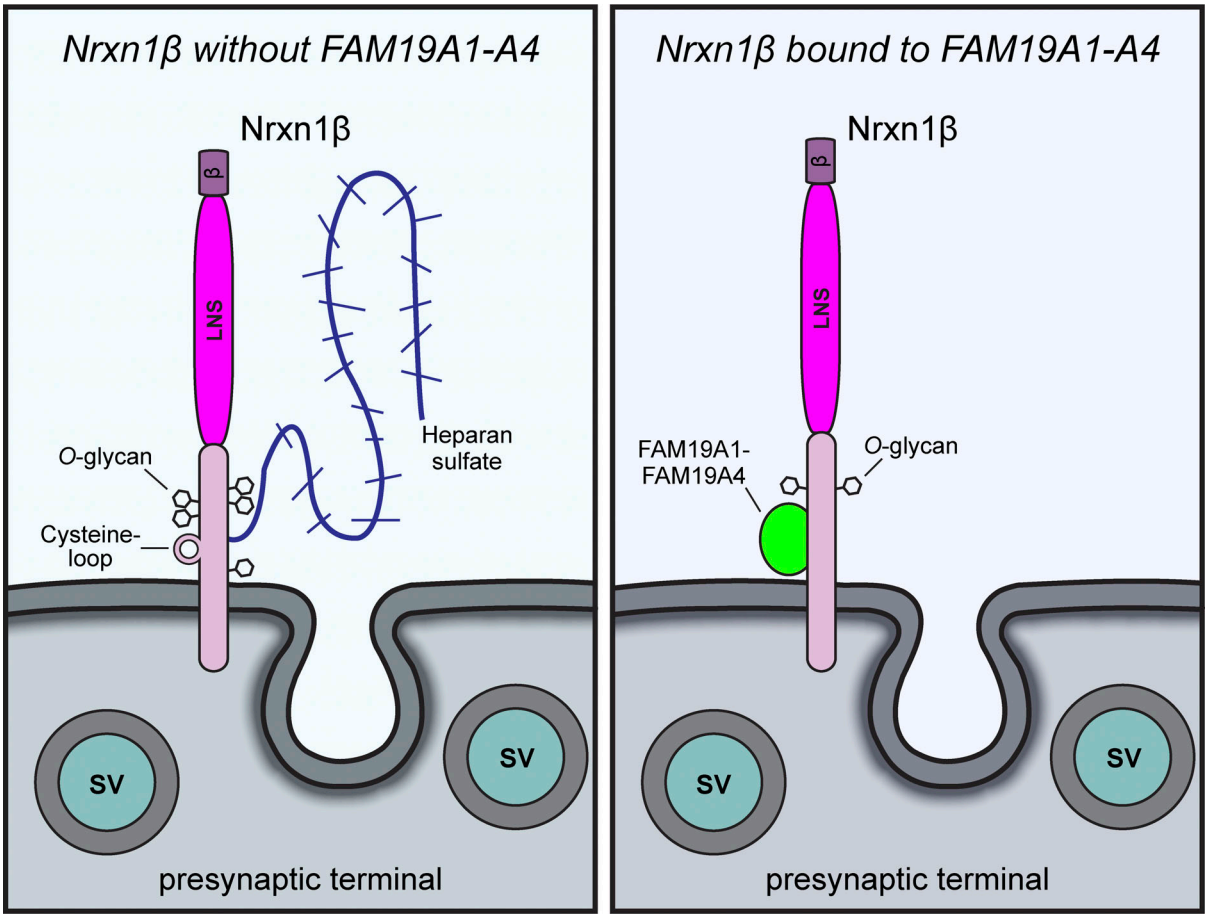

Figure 10. **A model of the regulation of neurexin post-translational modifications by FAM19A1-A4**. The schematic depicts a presynaptic terminal containing Nrxn1β as an exemplary neurexin isoform that was exported to the cell surface either in the absence (left) or presence (right) of FAM19A1-A4. Binding of FAM19A1-A4 early in the secretory pathway down-regulates subsequent modifications by *O*-glycans or heparan sulfate. β, β-Nrxn-specific sequence; LNS, sixth LNS domain that is the only LNS-domain of β-neurexins; SV, synaptic vesicles.

(Fig. 6, Fig. 7, and Fig. 8; Chen et al., 2017) or CD-1 mice (Fig. 9). The hippocampi of pups were dissected and mixed, regardless of gender. Hippocampi were dissected in ice-cold HBSS and kept on ice until digestion with 0.2 µm-filtered 10 U/ml papain (Worthington Biochemical Corporation) in HBSS in a 37°C water bath for 20 min. Hippocampi were washed twice with HBSS and once with plating medium (MEM [Gibco] supplemented with 2 mM L-glutamine [Gibco], 0.4% glucose [Sigma-Aldrich], 2% Gem21 NeuroPlex Serum-Free Supplement [Gemini], and 5% FBS [Atlanta]). Cells were dissociated in plating media and plated onto autoclaved glass coverslips coated with Matrigel Membrane Matrix (Corning) in 24-well plates (one pup's hippocampi/12 wells). This day was considered DIV0. On DIV1, 80% of the plating medium was replaced with fresh, prewarmed growth medium (Neurobasal-A [Gibco] supplemented with 2% Gem21 NeuroPlex Serum-Free Supplement and 2 mM L-glutamine [Sigma-Aldrich]). At DIV3–4, when glia were nearly confluent, 50% of the medium was replaced with fresh, prewarmed plating medium and a final concentration of 2 µM cytosine arabinoside. At DIV8, 50% of the medium was replaced with fresh, prewarmed plating medium. Analyses were performed at DIV14–16.

Nrxn123 cKO hippocampal cultures

At DIV4, hippocampal cultures were infected with lentiviruses encoding Cre or ΔCre. At DIV6, hippocampal cultures were infected with control lentiviruses or lentiviruses encoding mouse FAM19A1-V5 (containing the endogenous FAM19A1 signal peptide).

Activity induction in hippocampal cultures

At DIV14, CD-1 hippocampal cultures underwent a 50% conditioned media swap yielding a final concentration of 100 µM picrotoxin or vehicle (0.1% DMSO). RNA was collected 2, 6, 24, and 48 h after treatment with picrotoxin or vehicle. Prior to lysis for RNA extraction, cells were washed once using ice-cold Dulbecco's phosphate-buffered saline (DPBS; Gibco).

HEK293T cells

HEK293T cells (ATCC CRL11268) were grown in complete DMEM (cDMEM), which consisted of DMEM (Gibco), 5% FBS (Sigma-Aldrich), penicillin, and streptomycin. All transfections were performed using calcium phosphate, either with a CalPhos Mammalian Transfection Kit (Takara) or reagents generated in-house. For coIP experiments, HEK293T cells were plated onto

21-cm^2 dishes. For immunocytochemistry and cell surface binding experiments, HEK293T cells were plated onto poly-L-lysine (150–300 kD; Sigma-Aldrich)–coated glass coverslips in 24-well plates. Medium was replaced with fresh, prewarmed cDMEM 1 h before transfection. Unless otherwise noted, cells were washed once with prewarmed DPBS, and medium was replaced with fresh, prewarmed cDMEM ∼12 h after transfection. Samples were collected ∼48 h after transfection.

Real-time quantitative RT-PCR (qRT-PCR)

For qRT-PCR experiments, RNA concentration was measured using a NanoDrop 1000 Spectrophotometer (Thermo Fisher Scientific), and 8 ng total RNA was used per reaction. Transcripts were probed using PrimeTime qPCR Probe Assays (Integrated DNA Technologies), which consist of two primers and one FAM-labeled, ZEN/IBFQ-quenched 5′ nuclease probe. The following predesigned assays were used (gene, assay ID): *Actb* (Mm.PT.51.14022423), *Arc* (Mm.PT.58.5865502.g), *Car10* (Mm.PT.58.11765793), *Car11* (Mm.PT.58.32895602), *Fam19a1* (Mm.PT.56a.6079538), *Fam19a2* (Mm.PT.58.7298614), *Fam19a4* (Mm.PT.56a.9330679), *Fam19a5* (Mm.PT.56a.8916996), *Fos* (Mm.PT.58.29977214), and *Gapdh* (4352932E, Applied Biosystems). Additionally, the following assays were used (gene, primer 1, primer 2, probe): *Nrxn1αβγ*, 5′-CGATGTCATCTGTCCCAACA-3′, 5′-GCCATCGGATTTAGCACT GTC-3′, 5′-TGGAGCTGCACATACACCAAGGAA-3′; *Nrxn2αβ*, 5′-TGATATTTGCCGTCGCTCAC-3′, 5′-GGTGCGAGTGGACAGTG-3′, 5′-TCAATTGTAATGTCGTCCGTGCCCA-3′; and *Nrxn3αβ*, 5′-CAC TGATAATGAACGCCTCCA-3′, 5′-CCTTTGTCCTTTCCTCCGATG-3′, 5′-CCTTTTTCCTGCAGCCACTCCTCT-3′. Assays generating threshold cycle (C_t) values >35 were omitted. C_t values for technical replicates differed by less than 0.5. C_t values were averaged for technical replicates.

Brain tissue

For qRT-PCR from brain tissue, dissections and RNA extraction were performed as described in Seigneur and Südhof (2017). VeriQuest Probe One-Step qRT-PCR Master Mix with ROX (Affymetrix) and an ABI 7900HT Fast RT-PCR instrument (Applied Biosystems) were used. Samples were run in technical triplicates with *Gapdh* and *Actb* as loading controls. Data were normalized to the arithmetic mean of *Gapdh* and *Actb*, and mean $2^{-\Delta Ct}$ values are plotted.

Hippocampal cultures

For qRT-PCR from hippocampal cultures, total RNA was isolated using a RNeasy Mini Kit (Qiagen) per the manufacturer's instructions. TaqMan Fast Virus 1-Step Master Mix (Thermo Fisher Scientific) and a QuantStudio 3 RT-PCR System (Thermo Fisher Scientific) were used, and samples were run in technical duplicates with *Gapdh* as a loading control. Additionally, data were normalized to the control group within each experimental replicate (vehicle 2 h post-treatment). Mean $2^{-\Delta\Delta Ct}$ values are plotted.

Lentivirus generation and infection

All lentiviral protein expression was driven by the human synapsin I promoter (Südhof, 1990). LV-*SynI*-Cre-EGFP and LV-*SynI*-ΔCre-EGFP were generated by the Janelia Viral Tools facility and added to Nrxn123 cKO hippocampal cultures at DIV4 (Kaeser et al., 2009). Control and mouse FAM19A1-V5 lentiviruses were generated as described in Trotter et al. (2019). Briefly, the medium of HEK293T cells was replaced with fresh cDMEM containing 25 µM chloroquine diphosphate (Sigma-Aldrich) 1 h before transfection. Cells were transfected with lentiviral long terminal repeat (LTR)-containing vectors encoding FAM19A1-V5 or control (empty vector) with helper plasmids pRSV-REV, pMDLg/gRRE, and pVSVG. 16–20 h later, cells were washed with DPBS, and the medium was replaced with neural culture growth media. 48 h after transfection, viral supernatant was collected, cleared by centrifugation at 1,500 *g* for 10 min, aliquoted, and stored at −80°C. Viral supernatant (25 µl/well) containing control or FAM19A1-V5 lentiviruses was added to Nrxn123 cKO hippocampal cultures on DIV6.

Electrophysiology

Experimenters were blind to the treatment groups during recordings and analysis.

Recordings

For electrophysiological recordings of hippocampal cultures at DIV14–16, a coverslip was placed in a recording chamber mounted onto an Axioskop FS-2 upright microscope (Zeiss) equipped with differential interference contrast (DIC) and fluorescence filters, as well as a light-emitting diode (LED) source. Coverslips were maintained at room temperature (RT). Recordings were performed with a two-channel Axoclamp 700B amplifier (Axon Instruments) and digitalized with a Digidata 1440 digitizer (Molecular Devices) controlled by Clampex 10.7 (Molecular Devices). Patch pipettes (resistance of 2.5–3.5 MΩ) were pulled using borosilicate glass (WPI) on a two-stage vertical puller (Narishige). Neurons were voltage-clamped at −70 mV. The recording chamber was continuously perfused with oxygenated (95% O_2, 5% CO_2) standard artificial cerebrospinal fluid containing (in mM) 119 NaCl, 2.5 KCl, 1.3 $MgCl_2$, 2.5 $CaCl_2$, 11 glucose, 1 NaH_2PO_4, and 26 $NaHCO_3$. For mEPSC recordings, the following internal solution was used (in mM): 135 cesium methanesulfonate, 8 NaCl, 10 Hepes, 2 ATP-Mg, 0.3 GTP-Na, 0.1 Spermine, 7 phosphocreatine, and 0.3 EGTA, 300 mOsm/l, pH 7.3, adjusted with CsOH). The external solution contained 1 µM tetrodotoxin (TTX; American Radiolabeled Chemicals) and 100 µM picrotoxin (Tocris Bioscience). For mIPSC recordings, the internal solution consisted of (in mM) 135 CsCl, 10 Hepes, 1 EGTA, 4 ATP-Na, and 0.4 GTP-Na, 300 mOsm/l, pH 7.3, adjusted with CsOH). The external solution contained 1 µM TTX (American Radiolabeled Chemicals), 10 µM 6-cyano-7-nitroquinoxaline-2,3-dione (CNQX; Tocris Bioscience), and 50 µM AP5 (Tocris).

Analysis

Miniature currents were detected and analyzed offline in Clampfit 11.0.3 (Molecular Devices) using template matching. A lowpass Gaussian 1 kHz filter was used. The first minute of the recording was excluded from analysis. Events <8 pA were excluded. Cells for which the axis resistance >15 MΩ, or for which

the mean amplitude and/or frequency were statistical outliers (mean ± 2× standard deviation), were removed. Both cumulative distributions and averages are shown. Specifically, the graphs in the inset of Fig. 6, E, F, K, and L, show the average of the amplitude and frequency of each sample and have been statistically compared using two-tailed unpaired *t* tests, as indicated in the figure legend. For mEPSC recordings, data in these graphs are means ± SEM of 33 and 37 cells recorded across six independent cultures; for mIPSC, data in these graphs are means ± SEM of 25 cells recorded across five independent cultures. For cumulative distributions, we plotted the amplitude and inter-event interval of single events across all recorded cells (180 events for all cells except for one cell, for which only 133 events could be scored). We used the standard approach of analyzing the same number of events for each cell in order to avoid biasing the analysis toward outliers. The cumulative distributions have been compared using the Kolmogorov–Smirnov test.

Coimmunoprecipitation (coIP) assays

All samples were kept on ice until the addition of Laemmli sample buffer. Proteins were eluted from beads using 2× Laemmli sample buffer containing either 200 mM dithiothreitol (DTT) or 20 mM tris(2-carboxyethyl)phosphine hydrochloride (TCEP) and heating at 65°C for 10 min. Samples were analyzed by SDS-PAGE.

coIP from HEK293T media

Approximately 6 h after transfection, cells were washed once with prewarmed DPBS, and the medium was replaced with 3 ml of prewarmed Freestyle 293 Expression Medium (Gibco). The medium was collected ∼48 h after transfection. Hepes (10 mM final concentration), EDTA (5 mM final concentration), and cOmplete, EDTA-free protease inhibitor (Roche) were added to each sample at collection. Samples were centrifuged at 1,500 *g* for 15 min at 4°C in a swingout, tabletop centrifuge to pellet floating cells, and the medium was transferred to a fresh tube. 200 µl of medium (input) was removed and stored at −80°C. 40 µl of 1:1 slurry of washed mouse anti-V5 agarose beads (Thermo Fisher Scientific, A7345) was added to each sample, and samples were rotated overnight at 4°C. Samples were centrifuged at 1,500 *g* for 7 min at 4°C, and the medium (flow through) was discarded. Beads were washed three or four times with ice-cold DPBS before elution.

coIP from HEK293T lysates

Prior to collection, cells were washed once using ice-cold DPBS and collected in 500 µl of ice-cold DPBS containing cOmplete, EDTA-free protease inhibitors. Samples were centrifuged at 3,000 rpm for 5 min at 4°C. The DPBS was removed, and cell pellets were resuspended in 200 µl coIP buffer (100 mM NaCl, 4 mM KCl, 2 mM Ca_2Cl, 2 mM $MgCl_2$, and 20 mM Tris-HCl, pH 7.4) containing 1% Triton X-100 (Sigma-Aldrich) and cOmplete, EDTA-free protease inhibitors. Samples were incubated on ice for 1 h and gently vortexed every 15 min. Samples were then centrifuged at 14,000 rpm for 15 min at 4°C, and the clarified lysate was collected. A fraction (input) was saved and stored at −80°C. For each sample, 150 µl cleared lysate was mixed with 450 µl of coIP buffer and 30 µl of 1:1 slurry of washed mouse anti-V5 or anti-HA agarose beads (A2095, Millipore). Samples were rotated overnight at 4°C. Beads were washed five times with coIP buffer containing 0.1% Triton X-100 before elution.

Immunocytochemistry

Surface labeling of HEK293T cells and hippocampal cultures

Plates were placed on ice, and cells were washed once with ice-cold DPBS. Cells were fixed using 4% paraformaldehyde in DPBS for 20 min at RT, washed three times with DPBS, blocked (5% normal goat serum [Sigma-Aldrich] in DPBS) for 1 h at RT, and incubated with primary antibodies in blocking solution overnight at 4°C. Coverslips were washed three times with DPBS, incubated with secondary antibodies in blocking solution for 1 h at RT, and washed three times with DPBS. HEK293T cell–containing coverslips were mounted onto positively charged glass slides using Fluoromount G without DAPI (Southern Biotech). Hippocampal cultures underwent total labeling (see below).

Total labeling of hippocampal cultures

Following surface labeling, hippocampal cultures were permeabilized in permeabilization/blocking buffer (0.2% Triton X-100 in blocking solution) for 1 h at RT, incubated with primary antibodies for total labeling in permeabilization/blocking buffer overnight at 4°C, washed three times with DPBS, incubated with secondary antibodies for total labeling in permeabilization/blocking buffer for 1 h at RT, washed three times with DPBS, and mounted onto positively charged glass slides using Fluoromount G without DAPI. The following primary antibodies were used: mouse anti-V5 (1:1,000; Invitrogen, R960-25, RRID: AB_2556564), chicken anti-microtubule-associated protein 2 (MAP2; 1:1,000; Aves Labs, MAP, RRID: AB_2313549), rabbit anti-vGluT1 (1:1,000; homemade, YZ6089), rabbit anti-vGAT (1:1,000; Millipore, AB5062P), and rabbit anti-HA (C29F4; 1:1,000; Cell Signaling, rabbit mAb 3724). The following Alexa Fluor Highly Cross-Adsorbed Secondary Antibodies (Invitrogen; raised in goat, IgG [Heavy + Light]) were used: anti-mouse 405 (1:500 or 1:1,000), anti-rabbit 405 (1:500 or 1:1,000), anti-mouse 546 (1:1,000), anti-rabbit 546 (1:1,000), and anti-chicken 647 (1:500 or 1:1,000).

Cell surface binding assay in HEK293T cells

Approximately 48 h after transfection, cells were washed three times with ice-cold Hepes bath buffer containing the following (in mM): 140–150 NaCl, 4–5 KCl, 2 $CaCl_2$, 1 $MgCl_2$, 10 glucose, and 10 Hepes, with the pH adjusted to 7.4 using NaOH [300 mOsm/l]). Next, cells were incubated in Hepes bath buffer with or without 100 nM FAM19A1-V5-His for 4 h at 4°C with gentle shaking. Cells were washed three times at 4°C with Hepes bath buffer, fixed, and surface labeled as described above.

Cell surface biotinylation of hippocampal cultures

All steps were performed on ice or at 4°C. Cells were washed twice with ice-cold DPBS containing 1 mM $MgCl_2$ and 0.1 mM $CaCl_2$ (DPBS+MC), then incubated with 1 mg/ml EZLink-Sulfo-NHS-SS-Biotin (in DPBS+MC; Thermo Fisher Scientific) at 4°C

for 30 min while gently shaking and protected from light. Cells were washed twice with quenching solution (100 mM glycine in DPBS+MC) for 10 min per wash with gentle shaking, then twice with PBS+MC. Cells were lysed in RIPA buffer (150 mM NaCl, 5 mM EDTA, 1% Triton X-100, 0.1% SDS, 25 mM Tris-HCl, pH 7.6) containing cOmplete, EDTA-free protease inhibitors (cRIPA; 50 µl/well). Lysate was centrifuged at 14,000 rpm for 15 min at 4°C. Cleared lysate was collected and stored at −80°C. 100–110 µl cleared lysate was used for experiments shown in Fig. 7. The total volume for the pull-down was brought up to 200 µl using cRIPA, and 35 µl of prewashed Dynabeads MyOne Streptavidin C1 (Thermo Fisher Scientific) was added to each sample. Samples were rotated at 4°C for 3 h. Flowthrough was saved, and beads were washed three times with cRIPA, then eluted using 2X Laemmli sample buffer (containing 200 mM DTT or 10 mM TCEP) at 65°C for 10 min. All samples were analyzed by SDS-PAGE.

Deglycosylation of cell surface proteins from hippocampal cultures

Cell surface proteins were purified as described above, except that equal amounts of total proteins were loaded across all groups within an experiment, the total volume for the pull-down was brought up to 300 µl, and 40 µl of prewashed Dynabeads MyOne Streptavidin C1 was added to each sample. Protein levels were measured using a BCA Protein Assay Kit (Pierce) per the manufacturer's instructions.

Removal of N- and O-linked glycans

After incubation of lysate with Dynabeads MyOne Streptavidin C1 beads, beads were washed twice with cRIPA, once with complete protein deglycosylation mix (cPDM) buffer (50 mM NaCl, 20 mM Tris-HCl, pH 7.5, and cOmplete, EDTA-free protease inhibitors) containing 1% Triton X-100, and once with cPDM buffer containing 0.2% Triton X-100. Deglycosylation Mix Buffer 2 (NEB), 10 mM TCEP, and cOmplete, EDTA-free protease inhibitors were added to the beads, and the samples were placed at 75°C for 10 min. Samples were briefly placed on ice. Protein Deglycosylation Mix II (NEB) was added, and samples were incubated at RT for 30 min. Next, samples were incubated at 37°C for 1 h with gentle shaking. Finally, Laemmli buffer (containing 200 mM DTT or 10 mM TCEP) was added, and samples were placed at 65°C for 10 min. The eluate was collected and stored at −80°C until evaluation by SDS-PAGE.

Removal of heparan sulfate (HS)

After incubation of lysate with Dynabeads MyOne Streptavidin C1 beads, beads were washed twice with cRIPA, once with Heparinase Reaction Buffer (NEB) containing 1% Triton X-100 and EDTA-free cOmplete protease inhibitors, and once with Heparinase Reaction Buffer containing 0.2% Triton X-100 and EDTA-free cOmplete protease inhibitors. *Bacteroides eggerthii* heparinases I, II, and III (1 µl of each, NEB) were added, in Heparinase Reaction Buffer containing 10 mM TCEP, 0.2% Triton X-100, and cOmplete, EDTA-free protease inhibitors, to each sample. Samples were incubated at 30°C for 2 h, with gentle shaking. Laemmli buffer (containing 200 mM DTT or 10 mM TCEP) was added to the samples, and they were placed at 65°C for 10 min. The eluate was collected and stored at −80°C until evaluation by SDS-PAGE.

Quantitative immunoblotting

4–20% Criterion TGX Precast Midi Protein gels (BioRad; 18-well, 30 µl) were used for all experiments except those shown in Fig. 8. For experiments shown in Fig. 8, 4–15% Criterion TGX Precast Midi Protein gels (BioRad; 12+2 well, 45 µl) were used. Proteins were transferred to a 0.2-µm-pore nitrocellulose membrane using a Criterion Blotter (BioRad) with plate electrodes, with transfer settings of 400 mV for 1.5 h at 4°C. The transfer buffer was composed of ice-cold Tris-glycine with 20% methanol. Membranes were blocked with 5% nonfat milk (Carnation) in Tris-buffered saline with 0.1% Tween-20 (TBST) for 1 h at RT, then incubated in primary antibody in blocking solution overnight (unless otherwise noted). Membranes were washed three times with TBST and incubated with secondary antibodies in blocking solution for 1 h at RT. Membranes were washed three times and scanned using an Odyssey CLx Imager (Li-COR) in automatic mode for dynamic range detection. When multiple antibodies were used, staining and scanning were done sequentially. Immunoblots were analyzed using free Image Studio Lite Version 5.2 (Li-COR). Channels were pseudo-colored using Adobe Photoshop CS (64-bit). Normalization was performed as described in the figure legends.

The following primary antibodies were used for immunoblotting: chicken anti-c-myc (1:500; Aves Labs, ET-MY100, RRID: AB_2313514), mouse anti-V5 (1:1,000; Invitrogen, R960-25, RRID: AB_2556564), rabbit anti-V5 (1:1,000; Millipore, AB3792), rabbit anti-Strep-tag II (1:1,000; Abcam, ab76949), rabbit anti-myc (clone 71D10; 1:1,000; Cell Signaling, rabbit mAb 2278), mouse anti-HA.11 (clone 16B12; 1:1,000; BioLegend, MMS-101R, RRID: AB_256533), mouse anti-GAPDH (clone 6C5; 1 h incubation at RT; 1:5,000; Millipore, MAB374), rabbit anti-pan-Nrxn (1–2 overnight incubation at 4°C; 1:1,000; Millipore, ABN161-I), mouse anti-$GABA_AR$ β2/3 (clone 62-3G1; 1:500; NeuroMab, 75–363, RRID: AB_2315837), mouse anti-Δ-HS (3G10 epitope, clone F69-3G10; 1:1,000; Amsbio, 370260-S), and rabbit anti-synapsin (1:1,000; homemade, YZ6079). The following secondary antibodies (Li-COR) were used (1:10,000 in blocking solution): IRDye 800CW donkey anti-mouse (926–32212; RRID: AB_2716622), IRDye 680LT donkey anti-mouse (926–68022; RRID: AB_2814906), IRDye 800CW donkey anti-rabbit (926–32213; RRID: AB_621848), and IRDye 680LT donkey anti-rabbit (926–68023; RRID: AB_10706167).

Identification of specific and non-specific bands in pan-neurexin immunoblots

Specific bands in pan-neurexin immunoblots were identified by their disappearance after neurexin deletion in Nrxn123 cKO hippocampal cultures infected with lentiviral Cre. Non-specific bands were identified based on their persistence, without a qualitative change in band intensity, after neurexin deletion in Nrxn123 cKO hippocampal cultures infected with lentiviral Cre.

Recombinant protein expression and purification for cell surface binding

400 ml of Expi293F cells (Gibco) at a density of 3 × 10^6 viable cells/ml were transfected using a ExpiFectamine 293 Transfection Kit (Gibco) per the Expi293 Expression System user guide instructions. 6 d later, one cOmplete, EDTA-free protease inhibitor tablet was added to the culture, and it was harvested. The cell culture suspension was centrifuged at 4,000 *g* for 30 min to pellet down cells. The medium was collected and the pH was adjusted to 8.0 using 20 mM (final concentration) Tris-HCl (pH 8.0). Imidazole was added to a final concentration of 10 mM. 5 ml of prewashed 1:1 HisPur Ni NTA resin (Thermo Fisher Scientific) in equilibration buffer consisting of 20 mM Tris-HCl, 300 mM NaCl (20/300 TBS), and 20 mM imidazole was added to the media. Batch binding was allowed to occur for 2 h at RT, with gentle stirring. The resin was collected and washed with ∼25 ml of 20/300 TBS containing 25 mM imidazole. Recombinant protein was eluted in 20 ml of 20/300 TBS containing 200 mM imidazole. The eluate was concentrated to 1 ml using a prewet centrifugal filtration unit containing a 3-kD molecular weight cut-off membrane (Amplicon). The sample was injected onto a Superdex 75 Increase 10/300 GL column (GE) connected to an NGC Quest 10 Chromatography System (BioRad) and eluted over 1 column volume (CV) using 20/300 TBS. Peak fractions were analyzed by Coomassie staining of non-reducing and reducing SDS-gels. The peak fraction corresponding to the FAM19A1-V5-His monomer was used for cell surface binding.

Recombinant protein expression and purification for size-exclusion chromatography coupled with multi-angle light scattering (SEC-MALS)

For recombinant protein expression for SEC-MALS, the BacMam system (Dukkipati et al., 2008; Goehring et al., 2014; Wilson et al., 2019) was used. Constructs were cloned into the pEG BacMam vector and transformed into MAX Efficiency DH10Bac Competent *Escherichia coli* (Invitrogen) to generate recombinant bacmid DNA. SF9 cells were transfected to generate BacMam viruses, which were then amplified. BacMam viruses were used to transduce HEK293S GnTI$^-$ cells (ATCC CRL-3022) or, in the case of FAM19A1-V5-6xHis, FreeStyle 293-F cells (Gibco; grown per the manufacturer's instructions) were used for protein expression. HEK293S GnTI$^-$ cells were grown in suspension in FreeStyle 293 Expression Medium (Gibco) containing 2% FBS at 37°C and with 8% CO_2. When the cell density reached 1–2 × 10^6 cells/ml, 1–2 liters of cell cultures were (1) cotransduced with BacMam viruses encoding Igκ signal peptide-Nrxn1β$^{SS4\text{-}SS5}$-ECD-Myc-6xHis and FAM19A1-V5 containing the endogenous signal peptide, or transduced with BacMam viruses encoding (2) Igκ signal peptide-Nrxn1β$^{SS4\text{-}SS5}$-ECD-Myc-6xHis, (3) Igκ signal peptide-FAM19A1-Twin-Strep, or (4) FAM19A1-V5-His containing the endogenous signal peptide. For the purification of the Nrxn1β-ECD-Myc-6xHis/FAM19A1-V5 complex, 1:2 volumes of supernatants containing the BacMam viruses were used for transduction. 10 mM sodium butyrate was added to the cultures 8–24 h after transduction, and the incubation temperature was lowered to 30°C. Approximately 72–96 h after transduction, cOmplete, EDTA-free protease inhibitors were added to the cell culture, cells were pelleted by centrifugation, and the medium was collected. At RT, medium was concentrated, and the buffer was exchanged into 20/150 TBS using a 10-kD membrane (Omega Centramate Pall T-series). For the purification of 6xHis-tagged proteins or protein complexes, this buffer also contained 10 mM imidazole. The resulting protein-containing solution was loaded onto 5 ml His Trap HP(GE) columns using an ÄKTA Start (GE) at 4°C. Columns were washed with a solution of 20/300 TBS containing 25 mM imidazole. 6xHis-tagged proteins/protein complexes were eluted using a 50–500-mM imidazole gradient (in 20/300 TBS) over 10 CV. Peak fractions were evaluated by Coomassie staining of reducing and non-reducing SDS-gels, and fractions of interest were combined and concentrated using a 3- or 10-kD-molecular-weight cut-off centrifugal filtration unit. Further purification steps were performed as described below, with columns attached to an ÄKTA pure purification system (GE). For the purification of Nrxn1β-ECD-Myc-6xHis, the immobilized metal affinity chromatography (IMAC)-purified protein solution was loaded onto a HiLoad 16/600 Superdex 200 PG column and eluted over 1 CV using 20/150 TBS. For the purification of the Nrxn1β-ECD-Myc-6xHis/FAM19A1-V5 complex, fractions of interest from IMAC were combined and dialyzed in 20/50 TBS. The resulting sample was loaded onto a Mono Q 4.6/100 OE column (GE), and the proteins of interest were eluted using a 30 CV gradient of 20/50 to 20/500 TBS. Fractions of interest were pooled and loaded onto a Superdex 200 10/300 GL column and eluted using 20/150 TBS. Fractions of interest were pooled, the sample was diluted such that the concentration of NaCl was 50 mM, and the sample was again loaded onto a Mono Q 4.6/100 OE column (GE). Proteins were eluted with a 40 CV gradient of 20/50 to 20/500 TBS. For the purification of FAM19A1-V5-6xHis, fractions of interest were pooled, loaded onto a Superdex 75 10/300 GL column, and eluted over 1.25 CV using 20/150 TBS. For the purification of FAM19A1-Twin-Strep, the concentrated, buffer-exchanged protein-containing solution was loaded onto StrepTrap HP columns (GE), washed with 20/150 TBS, and batch-eluted using 2.5 mM desthiobiotin (Sigma-Aldrich) in 20/150 TBS. The eluate was concentrated and loaded onto either a Superdex 75 10/300 GL column (GE) or a HiLoad Superdex 75 PG column for small- and large-scale purification, respectively. Protein concentration measurements were performed using a NanoDrop 1000 spectrophotometer (Thermo Fisher Scientific), with the expected molecular weights and extinction coefficients taken into account.

Other recombinant protein expression and purification

For experiments shown in Fig. 4 A, Igκ-Nrxn1β-ECD-Myc-6xHis and FAM19A1-V5 were coexpressed in FreeStyle 293-F cells transfected using polyethylenimine. The recombinant Nrxn1β-ECD/FAM19A1 complex was purified from the medium by batch elution of bound Nrxn1β-ECD from a TALON column, followed by SEC on a Superdex 200 column.

SEC-MALS

200 µl of ∼1 mg/ml purified recombinant protein was used for SEC-MALS. For the Nrxn1β-ECD/FAM19A1 complex and

Nrxn1β-ECD, a Superdex 200 10/300 GL column (GE) was used. For FAM19A1-Twin-Strep, a Superdex 75 10/300 GL column (GE) was used. The flow rate was 0.5 ml/min in PBS, pH 7.4 (Sigma-Aldrich). Using Dawn Heleos-II and Optilab rEX instruments (Wyatt Technology), UV absorption at 280 nm, light scattering, and differential refractometry data were recorded for protein elution profiles. A bovine serum albumin reference was used to correct the baseline. Data analyses were performed using ASTRA 7.1.2 (Wyatt Technology). A differential refractive index increment (dn/dc) value of 0.185 was used for all calculations.

Absolute mass determination by mass spectrometry

Absolute mass determination was performed by the Stanford University Mass Spectrometry core. Samples were analyzed, as provided, by electrospray ionization mass spectrometry on the Agilent 1260 HPLC and Bruker MicroTOF-Q II. Solvent A consisted of 0.05% trifluoroacetic acid (TFA) and 0.09% formic acid in water, and Solvent B consisted of 0.1% formic acid in acetonitrile. The gradient was as follows (time in minutes, Solvent A, Solvent B): 0–1.5, 95%, 5%; 2, 65%, 35%; 10, 54%, 46%; 11–12, 5%, 95%; 13, 95%, 5%. The column was an Agilent Pursuit 5 diphenyl 150 × 2.1 mm, the temperature was 80°C, and the flow rate was 0.3 ml/min. The volume injected was 5 µl. Data were collected in full-scan MS mode with a mass range of 400–4,000 D. The collision radio frequency (RF) setting was 800 Vpp.

Confocal microscopy and analysis

The experimenter was blind to the treatment groups during image acquisition and analysis.

Image acquisition

Confocal images were acquired at RT using an inverted Nikon A1Rsi Eclipse Ti confocal microscope (Nikon) operated by NIS-Elements AR acquisition software (Nikon). All images were 1,024 × 1,024 pixels. When multiple channels were used, images in each channel were acquired sequentially to avoid bleed-through. The same imaging settings were used throughout for all groups within an experimental replicate and were optimized to prevent pixel saturation. All images for a given experimental replicate were acquired on the same day with the same acquisition settings. Positive and negative control groups were included within each experimental replicate.

HEK293T cells

Confocal images of HEK293T cells were acquired using a 20× objective, 3.46× digital zoom, and a z-stack distance of 2 µm. Fields of view were chosen using the EGFP signal only.

Hippocampal cultures

Confocal images of hippocampal cultures were acquired using a 60× oil objective (Apo, NA 1.4), 1.82× digital zoom, and a z-stack distance of 0.5 µm. Neurons were selected based on health (i.e., MAP2 integrity) based on the MAP2 signal alone.

Analysis

Confocal image analysis was performed using NIS-Elements Advanced Research software (Nikon). Maximum intensity projections were generated and analyzed, and are depicted in representative images. All images acquired within the same day underwent equal background subtraction before analysis. For synapse analysis, 20–40 µm lengths of secondary or tertiary dendrites (no intersecting dendrites) were quantified per neuron, with 9–13 neurons analyzed per experiment (n = 4 independent cultures). These regions of interest were drawn solely based on MAP2 staining. Excitatory and inhibitory synapses were defined as vGluT1- or vGAT-positive puncta associated with MAP2, respectively, using the General Analysis function. Puncta density, area, and mean intensity were averaged per independent culture before statistical analysis. Mean intensity values were normalized to the control group within each independent culture.

Statistical analyses

Statistical analyses were performed using GraphPad Prism 8 software as described in the figure legends.

Online supplemental material

Fig. S1 shows expression of *Fam19a* mRNAs in different brain regions as a function of development and cell type in mouse brain. Fig. S2 shows that FAM19A1-A4, but not FAM19A5, binds to all neurexin isoforms and splice variants tested as assessed by the neurexin-mediated exposure of FAM19A proteins on the surface of HEK293T cells coexpressing the various FAM19A proteins and neurexins. Fig. S3 shows that exogenously added FAM19A1 protein binds weakly to surface β-neurexin, in contrast to coexpressed FAM19A1 protein, which binds stoichiometrically, and purified recombinant FAM19A1 exists as a monomer as well as disulfide-mediated dimers. Fig. S4 shows that FAM19A1 binding to Nrxn1β is dependent on the cysteine residues in the neurexin Cys-loop domain, but the Cys-loop domain is insufficient for FAM19A1 binding since FAM19A1 does not bind to Nrxn1γ, which contains the Cys-loop domain, whereas CA10 does bind to Nrxn1γ. Fig. S5 shows that the deletion of neurexins decreases levels of surface-exposed FAM19A1 localized adjacent to dendrites but has no effect on the intrinsic electrical properties of neurons. It shows quantification of Nrxn123 deletion in Nrxn123 cKO mouse hippocampal cultures used in cell surface biotinylation experiments and assessment of the HS modification of neurexins using HS removal by treatment with heparinases.

Acknowledgments

We thank S.C. Wilson, R.A. Pfuetzner, J.H. Trotter, E.M. Seigneur, Z. Liu, K.J. Gan, and K.A. Raju (Stanford University School of Medicine, Stanford, CA) for advice and reagents.

This study was supported by grants from the National Institutes of Health (MH052804 to T.C. Südhof and R37MH63105 to A.T. Brunger) and the Deutsche Forschungsgemeinschaft (EXC 2189, 390939984 to B. Fakler). A.J. Khalaj was supported by a National Science Foundation Graduate Research Fellowship (DGE-114747).

The authors declare no competing financial interests.

Author contributions: A.J. Khalaj, F.H. Sterky, B. Fakler, and T.C. Südhof designed the experiments. A.J. Khalaj performed all

experiments except for the proteomic screen, which was performed by F.H. Sterky and J. Schwenk, and the electrophysiological recordings, which were performed by A. Sclip. All authors analyzed the data, and A.J. Khalaj and T.C. Südhof wrote the paper with input from all authors.

Submitted: 21 April 2020
Revised: 1 June 2020
Accepted: 5 June 2020

References

Anderson, G.R., J. Aoto, K. Tabuchi, C. Földy, J. Covy, A.X. Yee, D. Wu, S.-J. Lee, L. Chen, R.C. Malenka, et al. 2015. β-Neurexins Control Neural Circuits by Regulating Synaptic Endocannabinoid Signaling. *Cell*. 162: 593–606. https://doi.org/10.1016/j.cell.2015.06.056

Aoto, J., D.C. Martinelli, R.C. Malenka, K. Tabuchi, and T.C. Südhof. 2013. Presynaptic neurexin-3 alternative splicing trans-synaptically controls postsynaptic AMPA receptor trafficking. *Cell*. 154:75–88. https://doi.org/10.1016/j.cell.2013.05.060

Aoto, J., C. Földy, S.M.C. Ilcus, K. Tabuchi, and T.C. Südhof. 2015. Distinct circuit-dependent functions of presynaptic neurexin-3 at GABAergic and glutamatergic synapses. *Nat. Neurosci*. 18:997–1007. https://doi.org/10.1038/nn.4037

Araç, D., A.A. Boucard, E. Özkan, P. Strop, E. Newell, T.C. Südhof, and A.T. Brunger. 2007. Structures of neuroligin-1 and the neuroligin-1/neurexin-1 β complex reveal specific protein-protein and protein-Ca2+ interactions. *Neuron*. 56:992–1003. https://doi.org/10.1016/j.neuron.2007.12.002

Bildl, W., A. Haupt, C.S. Müller, M.L. Biniossek, J.O. Thumfart, B. Hüber, B. Fakler, and U. Schulte. 2012. Extending the Dynamic Range of Label--free Mass Spectrometric Quantification of Affinity Purifications. Mol. Cell. Proteomics. 11: M111.007955.

Brockhaus, J., M. Schreitmüller, D. Repetto, O. Klatt, C. Reissner, K. Elmslie, M. Heine, and M. Missler. 2018. α-Neurexins Together with α2δ-1 Auxiliary Subunits Regulate Ca^{2+} Influx through $Ca_v2.1$ Channels. *J. Neurosci*. 38:8277–8294. https://doi.org/10.1523/JNEUROSCI.0511-18.2018

Chen, L.Y., M. Jiang, B. Zhang, O. Gokce, and T.C. Südhof. 2017. Conditional Deletion of All Neurexins Defines Diversity of Essential Synaptic Organizer Functions for Neurexins. *Neuron*. 94:611–625.e4. https://doi.org/10.1016/j.neuron.2017.04.011

Choi, J.-H., Y.-M. Jeong, S. Kim, B. Lee, K. Ariyasiri, H.-T. Kim, S.-H. Jung, K.-S. Hwang, T.-I. Choi, C.O. Park, et al. 2018. Targeted knockout of a chemokine-like gene increases anxiety and fear responses. *Proc. Natl. Acad. Sci. USA*. 115:E1041–E1050. https://doi.org/10.1073/pnas.1707663115

Dai, J., J. Aoto, and T.C. Südhof. 2019. Alternative Splicing of Presynaptic Neurexins Differentially Controls Postsynaptic NMDA and AMPA Receptor Responses. *Neuron*. 102:993–1008.e5. https://doi.org/10.1016/j.neuron.2019.03.032

Delfini, M.C., A. Mantilleri, S. Gaillard, J. Hao, A. Reynders, P. Malapert, S. Alonso, A. François, C. Barrere, R. Seal, et al. 2013. TAFA4, a chemokine-like protein, modulates injury-induced mechanical and chemical pain hypersensitivity in mice. *Cell Rep*. 5:378–388. https://doi.org/10.1016/j.celrep.2013.09.013

Dukkipati, A., H.H. Park, D. Waghray, S. Fischer, and K.C. Garcia. 2008. BacMam system for high-level expression of recombinant soluble and membrane glycoproteins for structural studies. *Protein Expr. Purif*. 62: 160–170. https://doi.org/10.1016/j.pep.2008.08.004

Goehring, A., C.-H. Lee, K.H. Wang, J.C. Michel, D.P. Claxton, I. Baconguis, T. Althoff, S. Fischer, K.C. Garcia, and E. Gouaux. 2014. Screening and large-scale expression of membrane proteins in mammalian cells for structural studies. *Nat. Protoc*. 9:2574–2585. https://doi.org/10.1038/nprot.2014.173

Gokce, O., and T.C. Südhof. 2013. Membrane-tethered monomeric neurexin LNS-domain triggers synapse formation. *J. Neurosci*. 33:14617–14628. https://doi.org/10.1523/JNEUROSCI.1232-13.2013

Han, K.A., J.W. Um, and J. Ko. (2019). Intracellular protein complexes involved in synapse assembly in presynaptic neurons. In Advances in Protein Chemistry and Structural Biology, pp. 347–373.

Hoffman, R.C., L.L. Jennings, I. Tsigelny, D. Comoletti, R.E. Flynn, T.C. Sudhof, and P. Taylor. 2004. Structural characterization of recombinant soluble rat neuroligin 1: mapping of secondary structure and glycosylation by mass spectrometry. *Biochemistry*. 43:1496–1506. https://doi.org/10.1021/bi035278t

Hrvatin, S., D.R. Hochbaum, M.A. Nagy, M. Cicconet, K. Robertson, L. Cheadle, R. Zilionis, A. Ratner, R. Borges-Monroy, A.M. Klein, et al. 2018. Single-cell analysis of experience-dependent transcriptomic states in the mouse visual cortex. *Nat. Neurosci*. 21:120–129. https://doi.org/10.1038/s41593-017-0029-5

Ichtchenko, K., T. Nguyen, and T.C. Südhof. 1996. Structures, alternative splicing, and neurexin binding of multiple neuroligins. *J. Biol. Chem*. 271: 2676–2682. https://doi.org/10.1074/jbc.271.5.2676

Jang, S., H. Lee, and E. Kim. 2017. Synaptic adhesion molecules and excitatory synaptic transmission. *Curr. Opin. Neurobiol*. 45:45–50. https://doi.org/10.1016/j.conb.2017.03.005

Johnston, P.A., and T.C. Südhof. 1990. The multisubunit structure of synaptophysin. Relationship between disulfide bonding and homo-oligomerization. *J. Biol. Chem*. 265(15):8869–8873. .

Kaeser, P.S., L. Deng, A.E. Chávez, X. Liu, P.E. Castillo, and T.C. Südhof. 2009. ELKS2α/CAST deletion selectively increases neurotransmitter release at inhibitory synapses. *Neuron*. 64:227–239. https://doi.org/10.1016/j.neuron.2009.09.019

Kasem, E., T. Kurihara, and K. Tabuchi. 2018. Neurexins and neuropsychiatric disorders. *Neurosci. Res*. 127:53–60. https://doi.org/10.1016/j.neures.2017.10.012

Kim, S., B. Lee, J.-H. Choi, J.-H. Kim, C.-H. Kim, and H.-S. Shin. 2017. Deficiency of a brain-specific chemokine-like molecule, SAM3, induces cardinal phenotypes of autism spectrum disorders in mice. *Sci. Rep*. 7: 16503. https://doi.org/10.1038/s41598-017-16769-5

Krueger-Burg, D., T. Papadopoulos, and N. Brose. 2017. Organizers of inhibitory synapses come of age. *Curr. Opin. Neurobiol*. 45:66–77. https://doi.org/10.1016/j.conb.2017.04.003

Lei, X., L. Liu, C.E. Terrillion, S.S. Karuppagounder, P. Cisternas, M. Lay, D.C. Martinelli, S. Aja, X. Dong, M.V. Pletnikov, et al. 2019. FAM19A1, a brain-enriched and metabolically responsive neurokine, regulates food intake patterns and mouse behaviors. *FASEB J*. 33:14734–14747. https://doi.org/10.1096/fj.201901232RR

Luo, F., A. Sclip, M. Jiang, and T.C. Südhof. 2020. Neurexins cluster Ca 2+ channels within the presynaptic active zone. *EMBO J*. 39. e103208.

Matsuda, K., and M. Yuzaki. 2011. Cbln family proteins promote synapse formation by regulating distinct neurexin signaling pathways in various brain regions. *Eur. J. Neurosci*. 33:1447–1461. https://doi.org/10.1111/j.1460-9568.2011.07638.x

Matsuda, K., T. Budisantoso, N. Mitakidis, Y. Sugaya, E. Miura, W. Kakegawa, M. Yamasaki, K. Konno, M. Uchigashima, M. Abe, et al. 2016. Transsynaptic Modulation of Kainate Receptor Functions by C1q-like Proteins. *Neuron*. 90: 752–767. https://doi.org/https://doi.org/10.1016/j.neuron.2016.04.001

Miller, P.S., and A.R. Aricescu. 2014. Crystal structure of a human GABAA receptor. *Nature*. 512:270–275. https://doi.org/10.1038/nature13293

Missler, M., W. Zhang, A. Rohlmann, G. Kattenstroth, R.E. Hammer, K. Gottmann, and T.C. Südhof. 2003. Alpha-neurexins couple Ca2+ channels to synaptic vesicle exocytosis. *Nature*. 423:939–948. https://doi.org/10.1038/nature01755

Park, M.Y., H.S. Kim, M. Lee, B. Park, H.Y. Lee, E.B. Cho, J.Y. Seong, and Y.S. Bae. 2017. FAM19A5, a brain-specific chemokine, inhibits RANKL-induced osteoclast formation through formyl peptide receptor 2. *Sci. Rep*. 7:15575. https://doi.org/10.1038/s41598-017-15586-0

Reissner, C., F. Runkel, and M. Missler. 2013. Neurexins. *Genome Biol*. 14:213. https://doi.org/10.1186/gb-2013-14-9-213

Ribic, A., and T. Biederer. 2019. Emerging Roles of Synapse Organizers in the Regulation of Critical Periods. *Neural Plast*. 2019. 1538137. https://doi.org/10.1155/2019/1538137

Roppongi, R.T., S.H. Dhume, N. Padmanabhan, P. Silwal, N. Zahra, B. Karimi, C. Bomkamp, C.S. Patil, K. Champagne-Jorgensen, R.E. Twilley, et al. 2020. LRRTMs Organize Synapses through Differential Engagement of Neurexin and PTPσ. *Neuron*. 106:108–125.e12. https://doi.org/10.1016/j.neuron.2020.01.003

Rudenko, G.. 2019. Neurexins - versatile molecular platforms in the synaptic cleft. *Curr. Opin. Struct. Biol*. 54:112–121. https://doi.org/10.1016/j.sbi.2019.01.009

Saunders, A., E.Z. Macosko, A. Wysoker, M. Goldman, F.M. Krienen, H. de Rivera, E. Bien, M. Baum, L. Bortolin, S. Wang, et al. 2018. Molecular Diversity and Specializations among the Cells of the Adult Mouse Brain. *Cell*. 174:1015–1030.e16. https://doi.org/10.1016/j.cell.2018.07.028

Schreiner, D., T.M. Nguyen, G. Russo, S. Heber, A. Patrignani, E. Ahrné, and P. Scheiffele. 2014. Targeted combinatorial alternative splicing generates brain region-specific repertoires of neurexins. *Neuron*. 84: 386–398. https://doi.org/10.1016/j.neuron.2014.09.011

Schwenk, J., D. Baehrens, A. Haupt, W. Bildl, S. Boudkkazi, J. Roeper, B. Fakler, and U. Schulte. 2014. Regional diversity and developmental dynamics of the AMPA-receptor proteome in the mammalian brain. *Neuron*. 84:41–54. https://doi.org/10.1016/j.neuron.2014.08.044

Seigneur, E., and T.C. Südhof. 2017. Cerebellins are differentially expressed in selective subsets of neurons throughout the brain. *J. Comp. Neurol.* 525: 3286–3311. https://doi.org/10.1002/cne.24278

Sterky, F.H., J.H. Trotter, S. Lee, C.V. Recktenwald, X. Du, B. Zhou, and P. Zhou. 2017. Correction for Sterky et al., Carbonic anhydrase-related protein CA10 is an evolutionarily conserved pan-neurexin ligand. *Proc. Natl. Acad. Sci. USA*. 114. E2984. https://doi.org/10.1073/pnas.1621321114

Südhof, T.C.. 1990. The structure of the human synapsin I gene and protein. *J. Biol. Chem*. 265:7849–7852.

Südhof, T.C.. 2017. Synaptic Neurexin Complexes: A Molecular Code for the Logic of Neural Circuits. *Cell*. 171:745–769. https://doi.org/10.1016/j.cell.2017.10.024

Südhof, T.C.. 2018. Towards an Understanding of Synapse Formation. *Neuron*. 100:276–293. https://doi.org/10.1016/j.neuron.2018.09.040

Tasic, B., Z. Yao, L.T. Graybuck, K.A. Smith, T.N. Nguyen, D. Bertagnolli, J. Goldy, E. Garren, M.N. Economo, S. Viswanathan, et al. 2018. Shared and distinct transcriptomic cell types across neocortical areas. *Nature*. 563:72–78. https://doi.org/10.1038/s41586-018-0654-5

Tom Tang, Y., P. Emtage, W.D. Funk, T. Hu, M. Arterburn, E.E.J. Park, and F. Rupp. 2004. TAFA: a novel secreted family with conserved cysteine residues and restricted expression in the brain. *Genomics*. 83:727–734. https://doi.org/10.1016/j.ygeno.2003.10.006

Treutlein, B., O. Gokce, S.R. Quake, and T.C. Südhof. 2014. Cartography of neurexin alternative splicing mapped by single-molecule long-read mRNA sequencing. *Proc. Natl. Acad. Sci. USA*. 111:E1291–E1299. https://doi.org/10.1073/pnas.1403244111

Trotter, J.H., J. Hao, S. Maxeiner, T. Tsetsenis, Z. Liu, X. Zhuang, and T.C. Südhof. 2019. Synaptic neurexin-1 assembles into dynamically regulated active zone nanoclusters. *J. Cell Biol*. 218:2677–2698. https://doi.org/10.1083/jcb.201812076

Uemura, T., S.-J. Lee, M. Yasumura, T. Takeuchi, T. Yoshida, M. Ra, R. Taguchi, K. Sakimura, and M. Mishina. 2010. Trans-synaptic interaction of GluRdelta2 and Neurexin through Cbln1 mediates synapse formation in the cerebellum. *Cell*. 141:1068–1079. https://doi.org/10.1016/j.cell.2010.04.035

Ushkaryov, Y.A., and T.C. Südhof. 1993. Neurexin III alpha: extensive alternative splicing generates membrane-bound and soluble forms. *Proc. Natl. Acad. Sci. USA*. 90:6410–6414. https://doi.org/10.1073/pnas.90.14.6410

Ushkaryov, Y.A., A.G. Petrenko, M. Geppert, and T.C. Südhof. 1992. Neurexins: synaptic cell surface proteins related to the alpha-latrotoxin receptor and laminin. *Science*. 257:50–56. https://doi.org/10.1126/science.1621094

Ushkaryov, Y.A., Y. Hata, K. Ichtchenko, C. Moomaw, S. Afendis, C.A. Slaughter, and T.C. Südhof. 1994. Conserved domain structure of beta-neurexins. Unusual cleaved signal sequences in receptor-like neuronal cell-surface proteins. *J. Biol. Chem*. 269:11987–11992.

Wang, W., T. Li, X. Wang, W. Yuan, Y. Cheng, H. Zhang, E. Xu, Y. Zhang, S. Shi, D. Ma, et al. 2014. FAM19A4 is a novel cytokine ligand of formyl peptide receptor 1 (FPR1) and is able to promote the migration and phagocytosis of macrophages. *Cell. Mol. Immunol*. 12:615–624.

Wang, Y., D. Chen, Y. Zhang, P. Wang, C. Zheng, S. Zhang, B. Yu, L. Zhang, G. Zhao, B. Ma, et al. 2018. Novel adipokine, FAM19A5, inhibits neointima formation after injury through sphingosine-1-phosphate receptor 2. *Circulation*. 138:48–63. https://doi.org/10.1161/CIRCULATIONAHA.117.032398

Wilson, S.C., K.I. White, Q. Zhou, R.A. Pfuetzner, U.B. Choi, T.C. Südhof, and A.T. Brunger. 2019. Structures of neurexophilin-neurexin complexes reveal a regulatory mechanism of alternative splicing. *EMBO J*. 38. e101603. https://doi.org/10.15252/embj.2019101603

Yong, H.J., N. Ha, E.B. Cho, S. Yun, H. Kim, J.-I. Hwang, and J.Y. Seong. 2020. The unique expression profile of FAM19A1 in the mouse brain and its association with hyperactivity, long-term memory and fear acquisition. *Sci. Rep*. 10:3969. https://doi.org/10.1038/s41598-020-60266-1

Zeisel, A., H. Hochgerner, P. Lönnerberg, A. Johnsson, F. Memic, J. van der Zwan, M. Häring, E. Braun, L.E. Borm, G. La Manno, et al. 2018. Molecular Architecture of the Mouse Nervous System. *Cell*. 174:999–1014.e22. https://doi.org/10.1016/j.cell.2018.06.021

Zhang, P., H. Lu, R.T. Peixoto, M.K. Pines, Y. Ge, S. Oku, T.J. Siddiqui, Y. Xie, W. Wu, S. Archer-Hartmann, et al. 2018. Heparan Sulfate Organizes Neuronal Synapses through Neurexin Partnerships. *Cell*. 174: 1450–1464.e23. https://doi.org/10.1016/j.cell.2018.07.002

Zheng, C., D. Chen, Y. Zhang, Y. Bai, S. Huang, D. Zheng, W. Liang, S. She, X. Peng, P. Wang, et al. 2018. FAM19A1 is a new ligand for GPR1 that modulates neural stem-cell proliferation and differentiation. *FASEB J*. 32:5874–5890. https://doi.org/10.1096/fj.201800020RRR

Supplemental material

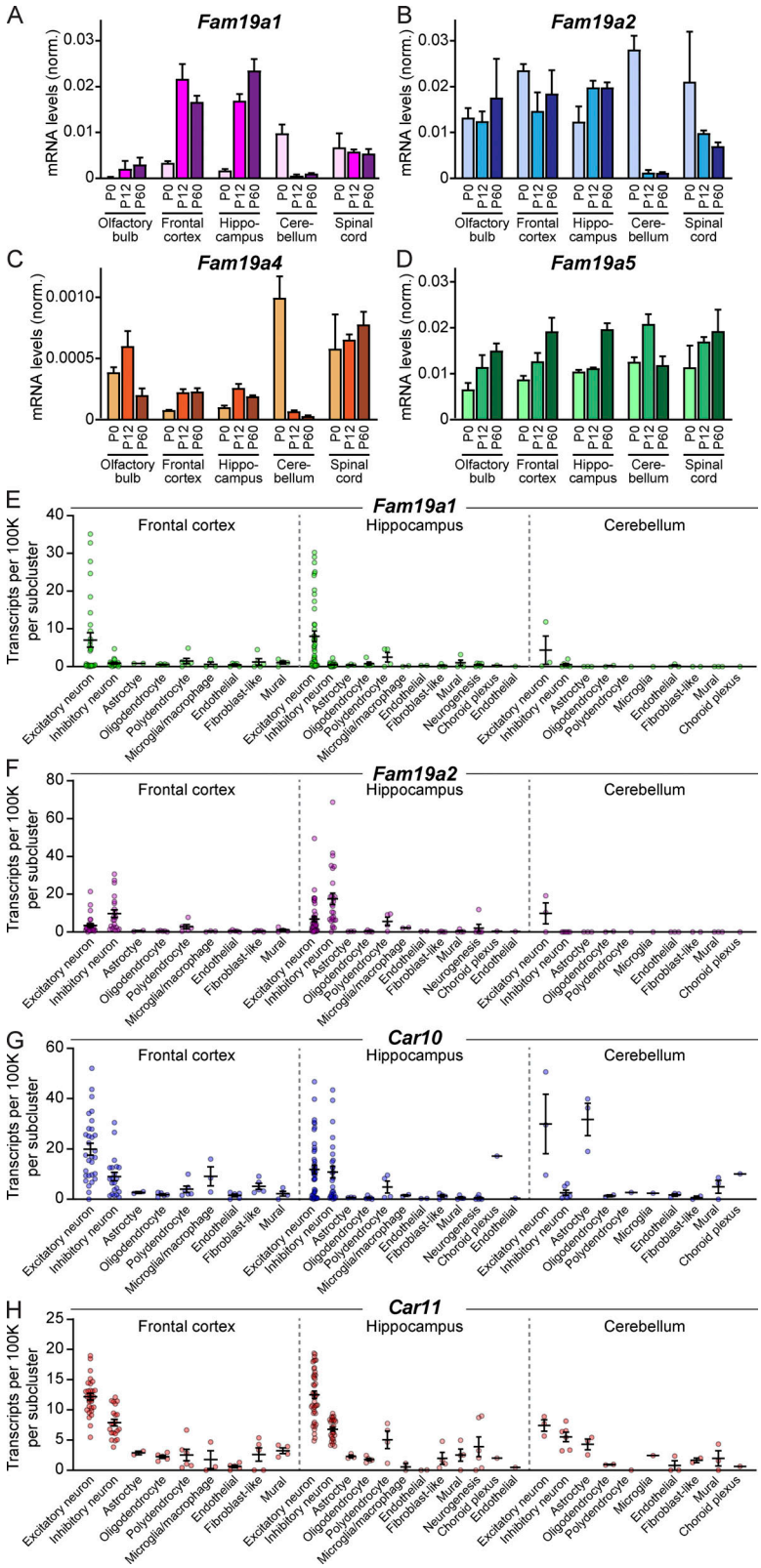

Figure S1. **Expression of *Fam19a* mRNAs in different brain regions as a function of development and cell type in mouse brain. (A–D)** mRNA levels for *Fam19a1* (A), *Fam19a2* (B), *Fam19a4* (C), and *Fam19a5* (D) as determined by quantitative RT-PCR of homogenates from the indicated brain regions dissected from newborn (post-natal day [P] 0), developing (P12), and young adult (P60) mice. *Fam19a3* mRNA was not detectable using two different qPCR assays and thus was not analyzed. Data are means ± SEM (n = 3 C57BL/6J male mice). Data are normalized to the arithmetic mean of *Actb* and *Gapdh*. **(E–H)** Single-cell RNA sequencing results for *Fam19a1* (E), *Fam19a2* (F), *Car10* (G), and *Car11* (H) from the frontal cortex, hippocampus, and cerebellum of adult male C57BL/6N mice (data from Saunders et al., 2018). Dots represent subclusters within cell type clusters. Data are means ± SEM.

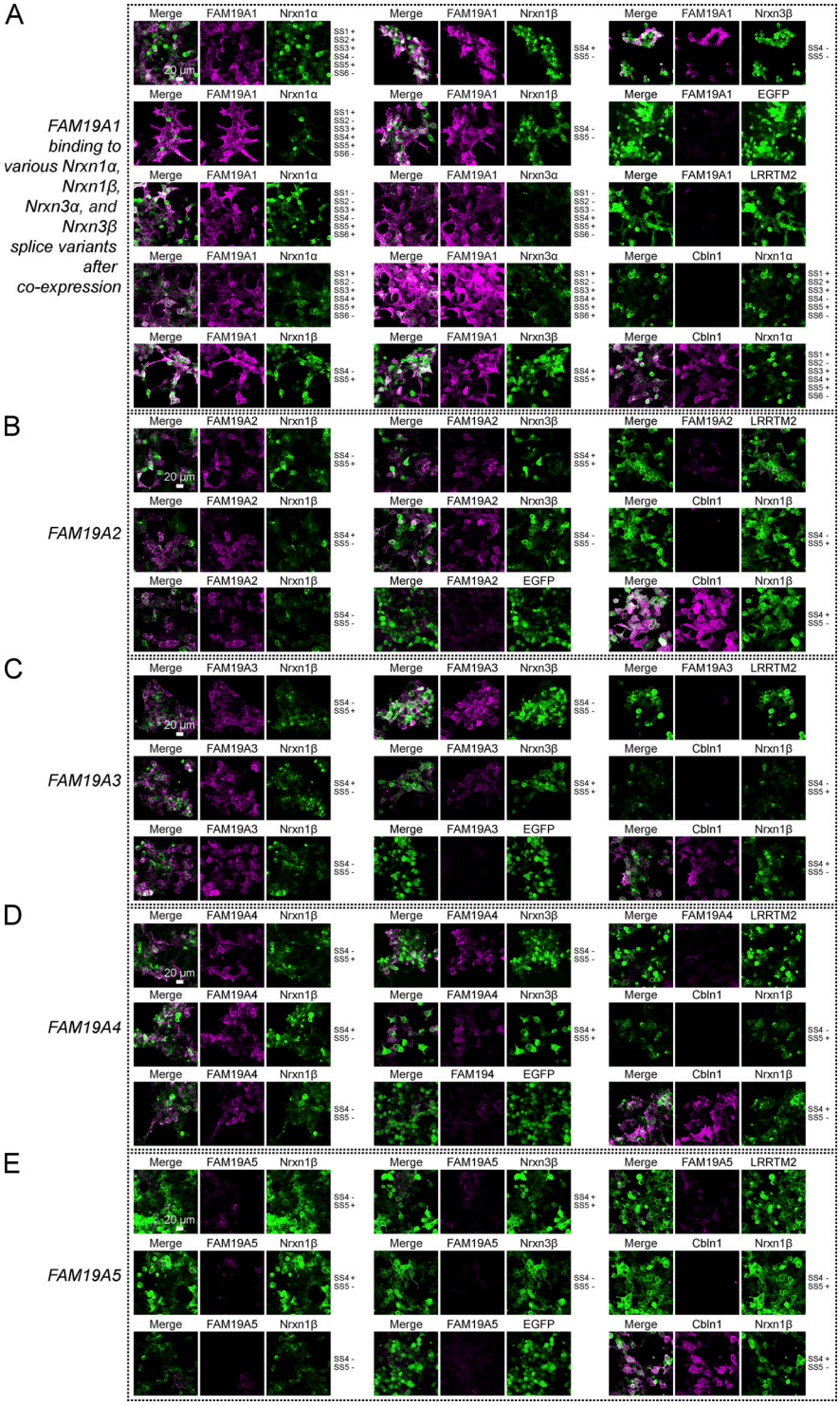

Figure S2. **FAM19A1-A4, but not FAM19A5, bind to all neurexin isoforms and splice variants tested as assessed by the neurexin-mediated exposure of FAM19A proteins on the surface of HEK293T cells coexpressing the various FAM19A proteins and neurexins. (A–E)** Representative images illustrating surface exposure of cerebellin-1 (Cbln1; A–E) or FAM19A1 (A), FAM19A2 (B), FAM19A3 (C), and FAM19A4 (D), but not FAM19A5 (E), with the indicated receptors in transfected HEK293T cells, as visualized by immunocytochemistry. These data complement those shown in Fig. 2 in that they depict additional neurexin splice variants and controls. Note that whereas Cbln1 only binds to the SS4^{+} variant of Nrxn1 (as expected), FAM19A1-A4 (but not FAM19A5) bind to both SS4^{-} and SS4^{+} variants of all neurexins tested, but not to LRRTM2 or EGFP-coexpressing HEK293T cells (negative controls). HEK293T cells were cotransfected with V5-tagged Cbln1 or FAM19A1-5 and the indicated EGFP-tagged Nrxn1 or Nrxn3 isoforms, EGFP-tagged LRRTM2, or EGFP. Surface labeling was performed for V5 (magenta), and compared with the EGFP signal (green). Panels show maximum intensity projections of representative confocal images taken at 20× magnification with 3.46× digital zoom. Images within each group were taken on the same day with the same acquisition settings, which were determined using the positive control group (Cbln1 coexpressed with Nrxn^{SS4+} variants). Scale bar, 20 µm. Images are representative of experiments independently replicated two to five times.

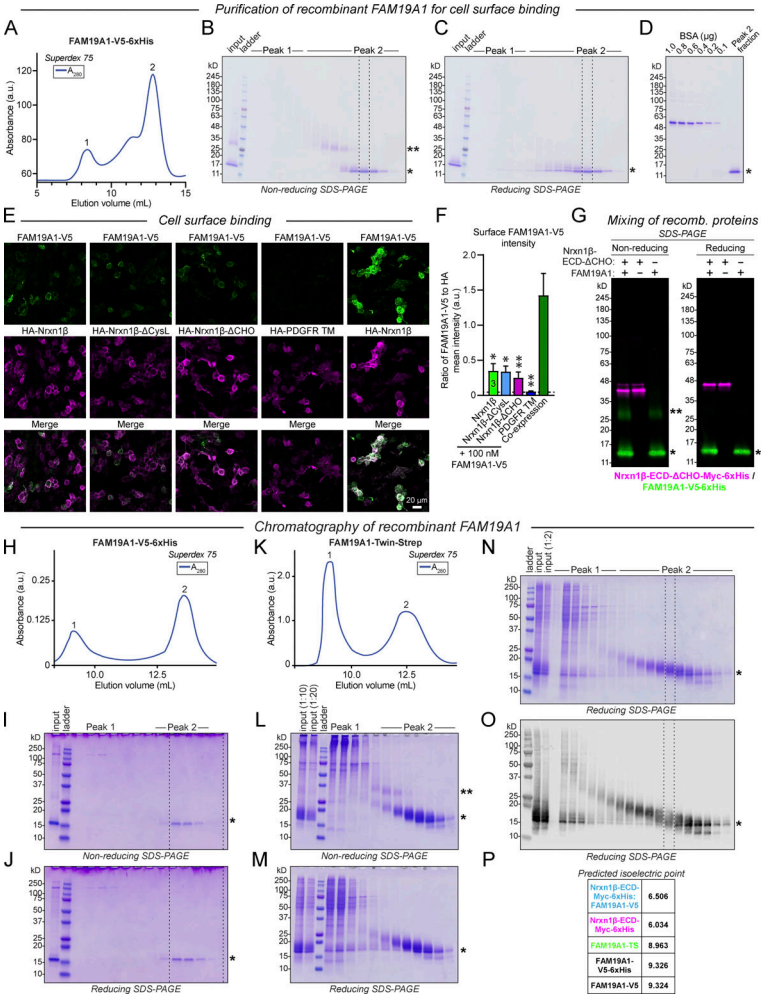

Figure S3. **Exogenously added FAM19A1 protein binds weakly to surface β-neurexin in contrast to coexpressed FAM19A1 protein that binds stoichiometrically, and purified recombinant FAM19A1 exists as a monomer as well as disulfide-mediated dimers. (A–D)** FAM19A1-V5-6xHis was purified from the medium of transfected Expi293 cells via pull-down using HisTrap followed by size-exclusion chromatography (SEC) on a Superdex 75 column (A). Fractions corresponding to peaks were analyzed by SDS-PAGE (B–D). The peak 2 fraction was found to exist as a monomer under non-reducing conditions and was used for subsequent cell surface binding assays. **, FAM19A1 homodimers; *, FAM19A1 monomers. **(E and F)** HEK293T cells were transfected with constructs encoding HA-tagged Nrxn1β, Nrxn1β-ΔCysL, Nrxn1β-ΔCHO (all Ser and Thr mutated to glycines to prevent *O*-glycosylation and HS modification), or the PDGFR transmembrane domain (TM). 48 h later, purified recombinant FAM19A1-V5-6xHis (A–D) was added at a final concentration of 100 nM for 4 h at 4°C to prevent endocytosis. Surface labeling was performed for V5 (green) and HA (magenta). In a separate condition, FAM19A1-V5 was coexpressed with Nrxn1β. The mean intensity of V5 pixels colocalized with HA pixels was normalized to the mean intensity of HA. Surface FAM19A1-V5 levels were lower when recombinant FAM19A1-V5 was added to Nrxn1β-, Nrxn1β-ΔCysL-, Nrxn1β-ΔCHO-, or PDGFR TM-expressing cells as compared with when FAM19A1-V5 and Nrxn1β were coexpressed (F). Data are means ± SEM (n = 3 independent experiments). Statistical analyses were performed using a repeated-measures one-way ANOVA with Tukey's post hoc test for multiple comparisons (*, $P < 0.05$; **, $P < 0.01$). **(G)** Purified recombinant (recomb.) Nrxn1β-ECD-ΔCHO-Myc-6xHis (Fig. 3, C, D, and G; magenta) was mixed with separately purified recombinant FAM19A1-V5-6xHis (A–D; green) for 4 h at 4°C and analyzed by non-reducing and reducing SDS-PAGE. Comigration was not observed under either condition. **, FAM19A1 homodimers; *, FAM19A1 monomers. **(H–J)** Purified recombinant FAM19A1 containing the endogenous signal peptide, as well as V5 and 6xHis tags, mostly exists as a monomer (*), with disulfide-mediated dimers detected in the input fraction in non-reducing (I), but not reducing (J), Coomassie-blue SDS-gels. Peak 2 consists of FAM19A1 monomers (H), while peak 1 likely contains an unspecific ∼150 kD protein. Monomeric purified recombinant FAM19A1 from fractions delineated by dotted lines (I and J) was used for absolute mass determination by ESI-MS (Fig. 3 I). FAM19A1-V5-6xHis was expressed in FreeStyle 293-F cells using the BacMam system. Recombinant FAM19A1 was purified by immobilized metal affinity chromatography (IMAC) followed by SEC on a Superdex 75 column. **(K–M)** Purified recombinant FAM19A1 in which the endogenous signal peptide was replaced with that of Igκ, and containing a Twin-Strep tag, exists as a monomer (*), with disulfide-mediated dimers (**) detected in the input fraction and within the left shoulder of Peak 2 in non-reducing (L), but not reducing (M), Coomassie-blue SDS-gels. Putatively, concentration-dependent disulfide-mediated multimers are detected within Peak 1 (L and M). Trial purification of recombinant FAM19A1-Twin-Strep shown in Fig. 3. Recombinant FAM19A1-Twin-Strep was expressed in HEK293S GnTI⁻ cells using the BacMam system and purified by batch elution from a StrepTactin column followed by SEC on a Superdex 75 column. **(N and O)** Side-by-side comparison of recombinant FAM19A1-Twin-Strep fractions analyzed by Coomassie-blue staining (N; same as in Fig. 3 F) and immunoblotting for Twin-Strep under reducing SDS-PAGE (O) confirms the predominance of FAM19A1 monomers within the input and the purity of FAM19A1 monomers within peak 2 (Fig. 3 F). It also supports the existence of disulfide-mediated FAM19A1 multimers within peak 1 (Fig. 3 F). **(P)** Predicted isoelectric points of the Nrxn1β-FAM19A1 complex and individual recombinant proteins shown in Fig. 3, Fig. 4 B, and Fig. S3 (Prot pi Protein Tool), which were used to inform the purification of the complex. Note that, for all proteins, it was assumed that all cysteines form disulfide bonds. For Nrxn1β, one $Man_5GlcNAc_2$ addition was assumed.

Predicted isoelectric point	
Nrxn1β-ECD-Myc-6xHis: FAM19A1-V5	6.506
Nrxn1β-ECD-Myc-6xHis	6.034
FAM19A1-TS	8.963
FAM19A1-V5-6xHis	9.326
FAM19A1-V5	9.324

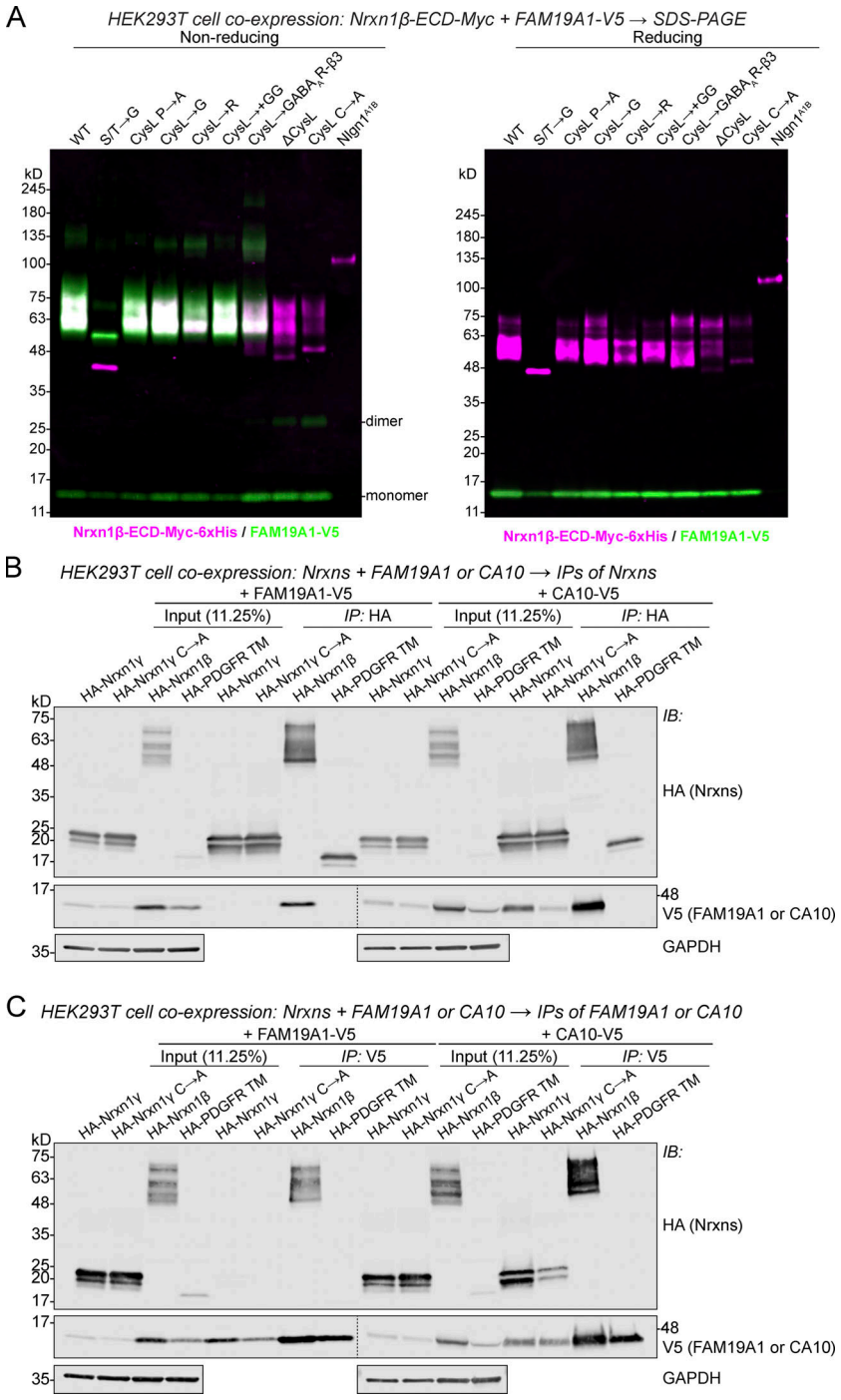

Figure S4. **FAM19A1 binding to Nrxn1β is dependent on the cysteine residues in the neurexin cysteine-loop domain, but the cysteine-loop domain is insufficient for FAM19A1 binding since FAM19A1 does not bind to Nrxn1γ that contains the cysteine-loop domain, whereas CA10 does bind to Nrxn1γ. (A)** Extended views of the immunoblots shown in Fig. 5 E. Under non-reducing conditions, FAM19A1 (green) comigrates (white) with all Nrxn mutants (magenta) shown here except when the Nrxn cysteine-loop (CysL) is deleted (ΔCysL) or the CysL cysteines are mutated (CysL C→A). The complexes are dissociated under reducing conditions. Further, disulfide-mediated FAM19A1 dimers are evident under non-reducing conditions when FAM19A1 is coexpressed with non-binding Nrxn mutants. Finally, FAM19A1 does not comigrate with Nlgn1, and FAM19A1 levels are relatively low when coexpressed with Nlgn1 (but detectable upon immunoprecipitation; see Fig. 5 D). **(B)** Coimmunoprecipitation (coIP) assays of HEK293T lysates demonstrate that HA-tagged Nrxn1γ does not bind to coexpressed V5-tagged FAM19A1, whereas it does bind to coexpressed CA10 (Sterky et al., 2017). Consistent with the dual requirement of the DILV sequence and the CysL domain in Nrxn for CA10 binding, Nrxn1γ lacking an intact CysL and CA10 coprecipitate more weakly than intact Nrxn1γ and CA10, suggesting that the DILV sequence is sufficient for some degree of binding. V5-tagged FAM19A1 or CA10 were coexpressed with the full-length wild-type (WT) or mutant Nrxn1γ, Nrxn1β (positive control), or the PDGFR transmembrane domain (TM; negative control) in HEK293T cells. Immunoprecipitation of HEK293T lysate was performed using HA antibodies and the immunoprecipitates were subjected to immunoblotting with antibodies to HA, V5, and GAPDH. Images depict representative blots from experiments that were independently replicated two times. **(C)** Same as B, except that the samples were immunoprecipitated with antibodies to V5. IB, immunoblot; IP, immunoprecipitation.

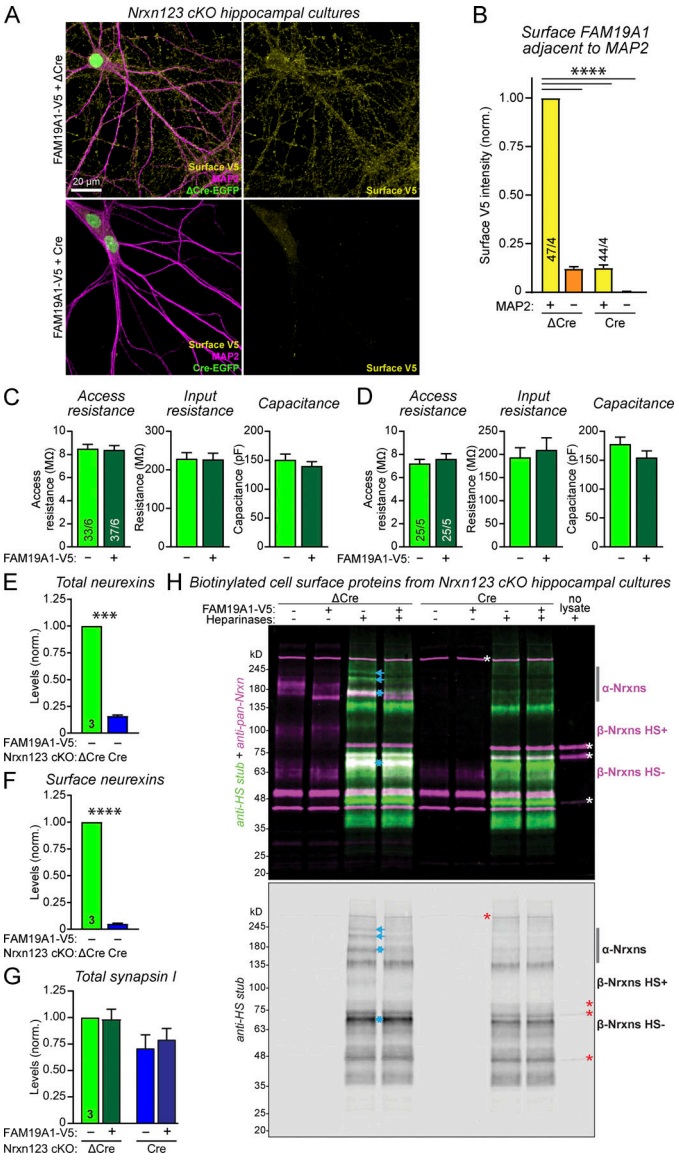

Figure S5. **The deletion of neurexins decreases levels of surface-exposed FAM19A1 localized adjacent to dendrites but has no effect on the intrinsic electrical properties of neurons. Quantification of Nrxn123 deletion in Nrxn123 cKO mouse hippocampal cultures used in cell surface biotinylation experiments and assessment of the heparan sulfate (HS) modification of neurexins using HS removal by treatment with heparinases. (A)** Hippocampal cultures prepared from Nrxn123 cKO mice were stained for surface-displayed FAM19A1-V5 (yellow) and for MAP2 (magenta). Green, EGFP signal produced by the lentivirally expressed EGFP-tagged Cre or ΔCre. **(B)** Quantification demonstrating that the vast majority of surface-displayed FAM19A1 puncta are adjacent to MAP2-positive dendrites, and that deletion of neurexins massively decreases the levels of all FAM19A1-positive puncta. The mean intensity of surface FAM19A1 adjacent to dendrites ($MAP2^+$) or not adjacent to dendrites ($MAP2^-$) was quantified in the presence of ΔCre or Cre expression in hippocampal cultures generated from newborn Nrxn123 cKO mice. Data are means of experimental replicates ± SEM (n = 4) independent cultures, with a total of 47 neurons analyzed for the ΔCre condition and 44 neurons analyzed for the Cre condition. Mean intensity values were normalized to the control group ($MAP2^+$, ΔCre) within each experimental replicate. Two-tailed one-sample t test (****, $P < 0.0001$). **(C and D)** Passive membrane properties from mEPSC (C) and mIPSC (D) recordings shown in Fig. 6. Means of cells ± SEM. Means were analyzed using a two-tailed unpaired t test. **(E–G)** Lentiviral expression of Cre-recombinase in hippocampal cultures from newborn Nrxn123 cKO mice causes an ∼80% reduction in total neurexin protein levels (E) and an ∼95% reduction in surface neurexin protein levels (F) in the absence of exogenously expressed FAM19A1, but neither exogenous expression of FAM19A1 nor deletion of neurexins have a significant effect on the total levels of synapsin I (G; see Fig. 7 A for representative immunoblots). Note that some of the neurexin signal detected in E and, to a much lesser extent in F, is attributable to non-specific bands detected by the pan-neurexin antibody (ABN161-I). Data are means ± SEM. Neurexin and synapsin I values are normalized to the loading control (GAPDH), followed by the control group (FAM19A1 negative, ΔCre) within each experimental replicate. n = 3 independent cultures, with at least three biological replicates pooled per condition. Two-tailed one-sample t test (***, $P < 0.001$; ****, $P < 0.0001$). **(H)** Top, double immunoblot of the membrane shown in Fig. 8 D using the anti-HS stub antibody (3G10, green) and a pan-neurexin antibody (ABN161-I, magenta) reveals four major overlapping bands (white) under the control condition, two of which are present when exogenous FAM19A1 is expressed. These bands are indicated by turquoise arrows. These data confirm the efficacy of treatment with heparinases and the reduction in HS-modified α-Nrxns when exogenous FAM19A1 is expressed. Bottom, immunoblot depicting HS-modified cell surface proteins from which HS has been removed. Differential banding due to exogenous FAM19A1 is obvious only when neurexins are present, suggesting that exogenous FAM19A1 does not affect the HS-modification of other HS-modified proteins.